PB-213 240

DEVELOPMENT AND APPLICATION OF TUNABLE DIODE LASERS TO THE DETECTION AND QUANTITATIVE EVALUATION OF POLLUTANT GASES

E. David Hinkley, et al

Massachusetts Institute of Technology

Prepared for:

Environmental Protection Agency

31 March 1972

DISTRIBUTED BY:

NTIS

National Technical Information Service
U. S. DEPARTMENT OF COMMERCE
5285 Port Royal Road, Springfield Va. 22151

PB 214 240

EPA-R2-72-090

Final Technical Report

Development and Application of Tunable Diode Lasers to the Detection and Quantitative Evaluation of Pollutant Gases

Prepared for Environmental Protection Agency
under Electronic Systems Division Contract F19628-70-C-0230 by

Lincoln Laboratory

MASSACHUSETTS INSTITUTE OF TECHNOLOGY

Lexington, Massachusetts

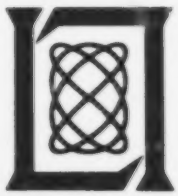

NATIONAL TECHNICAL
INFORMATION SERVICE

BIBLIOGRAPHIC DATA SHEET	1. Report No. EPA-R2-72-090	2.	3. Recipient's Accession No.
4. Title and Subtitle Development and Application of Tunable Diode Lasers to the Detection and Quantitative Evaluation of Pollutant Gases			5. Report Date March 31, 1972 6.
7. Author(s) E. D. Hinkley, J. O. Sample, et al			8. Performing Organization Rept. No.
9. Performing Organization Name and Address LINCOLN LABORATORY Massachusetts Institute of Technology Lexington, Massachusetts			10. Project/Task/Work Unit No. 11. Contract/Grant No.
12. Sponsoring Organization Name and Address ENVIRONMENTAL PROTECTION AGENCY National Environmental Research Center Division of Chemistry and Physics Research Triangle Park, N. C. 27711			13. Type of Report & Period Covered Final 14.

15. Supplementary Notes

Air Force Contract F19628-70-C-0230

16. Abstracts

The results are presented of a program concerned with the development of tunable semiconductor diode lasers and their potential application toward solving some of the air pollution monitoring problems. The tunable diode lasers developed under this program are described in Section 2. Section 3 contains some of the spectroscopic information obtained from the laser scans of portions of the gamma 1 band of SO_2 between 1100 and 1200 cm^{-1}, with special attention to comparison between experiment and theory. Initial experiments confirming the theory for remote heterodyne detection are described in Section 4. Section 5 consists of experiments related to potential monitoring applications involving tunable lasers. The use of the first and second derivative techniques in point-sampling applications is compared, and an experiment showing present limits of detectability is described. Preliminary studies of interference effects, temperature and long-path transmission of diode radiation are also included.

17. Key Words and Document Analysis. 17a. Descriptors

Air pollution
Lasers
Semiconductor lasers
Diodes
Exhaust gases
Flue gases
Sulfur dioxide
Remote sensing
Spectroscopy
Demodulation
Monitoring
Line spectra

17b. Identifiers/Open-Ended Terms

Air pollution detection

17c. COSATI Field/Group 13B

18. Availability Statement	19. Security Class (This Report)	21. No. of Pages
Unlimited	UNCLASSIFIED	65
	20. Security Class (This Page) UNCLASSIFIED	22. Price $3.00

FORM NTIS-35 (REV. 3-72)
THIS FORM MAY BE REPRODUCED
USCOMM-DC 14952-P72

EPA-R2-72-090

MASSACHUSETTS INSTITUTE OF TECHNOLOGY
LINCOLN LABORATORY

DEVELOPMENT AND APPLICATION OF TUNABLE DIODE LASERS TO THE DETECTION AND QUANTITATIVE EVALUATION OF POLLUTANT GASES

E. David Hinkley
Principal Investigator

FINAL TECHNICAL REPORT

ISSUED 31 MARCH 1972

Prepared for
Environmental Protection Agency
National Environmental Research Center
Division of Chemistry and Physics
Research Triangle Park, North Carolina

EPA Project Officer: John S. Nader

LEXINGTON MASSACHUSETTS

The work reported in this document was performed at Lincoln Laboratory, a center for research operated by Massachusetts Institute of Technology, with the support of the Environmental Protection Agency under Air Force Contract F19628-70-C-0230.

CONTENTS

Section		Page
	Summary	v
1.	INTRODUCTION	1
2.	DIODE LASER FABRICATION	3
3.	LASER SPECTROSCOPY OF SULFUR DIOXIDE	5
4.	REMOTE HETERODYNE DETECTION	9
	4.1 Heterodyne Theory and Calculations	10
	4.2 Heterodyne Detection of Thermal Radiation – Test of Theory	12
	4.3 Local Oscillator Power Requirement	15
	4.4 Heterodyne Detection of Ethylene	15
5.	EXPERIMENTS RELATED TO MONITORING APPLICATIONS OF TUNABLE LASERS	18
	5.1 Point Sampling Sensitivity Measurement	18
	5.2 Pressure, Temperature, and Interference Effects	19
	5.3 Long-Path Transmission Experiment	22
	Acknowledgments	23
	References	24
Appendix A:	Tunable Laser Spectra of the ν_1 Band of Sulfur Dioxide	25
Appendix B:	Tabulation of Sulfur Dioxide Spectral Data	37
Appendix C:	NH_3 Calibration Lines for the 1100-1200 cm^{-1} Region	42
Appendix D:	Detection of Air Pollutants with Tunable Diode Lasers	43
	References	51
Appendix E:	Tunable Laser Spectroscopy of the ν_1 Band of SO_2	53
	References	57

The work reported here was performed by

E. D. Hinkley

J. O. Sample

T. E. Stack

A. Wilson

J. H. Boghos*

S. Duda*

W. F. McBride*

J. N. McMillan*

W. H. Laswell*

R. J. Woods*

* Denotes part time.

SUMMARY

The purpose of this program is to develop and apply tunable semiconductor diode lasers to problems associated with the monitoring of pollutant gases. During the initial phase of the program, reported herein, lasers were developed to operate in the 8.7-μm region where sulfur dioxide (SO_2) has a strong infrared absorption band. Because of the potential usefulness of this band for various infrared techniques for the detection of SO_2, ultra-high-resolution laser scans were used to catalog several hundred of the spectral lines at reduced pressure. A theoretical spectrum for this band of SO_2, derived elsewhere on the basis of accurate microwave spectra, was found to be in near perfect agreement with the observed laser spectra once the band center used in the theory was properly adjusted on the basis of the laser data. We can now predict most of the strong SO_2 lines in this region, and construct with reasonable accuracy the absorption or emission spectrum of this gas corresponding to anticipated conditions of temperature, pressure, and instrumental resolution. Such information can be used, for example, to determine the optimum wavelength for the detection of SO_2 by across-the-stack absorption of laser radiation, over a wide temperature range. If such data were known for other constituent gases as well, particularly in the desired spectral region, a complete model could be used to facilitate development of suitable monitoring instrumentation. However, no such theories are available as yet.

Although the above theory contains the temperature dependence explicitly, it must rely on independent measurements for predictions involving pressure broadening of the lines. The rate of pressure broadening of SO_2 lines by air was measured by laser spectroscopy and found to be 12 MHz/Torr for the full width at half-maximum (FWHM); this yields an atmospheric-pressure-broadened linewidth of 0.30 cm^{-1}. Similar measurements for ammonia (NH_3) in the 10-μm region produce values of 6.3 MHz/Torr and 0.16 cm^{-1}, respectively.

Experiments were performed to verify the fundamental theory related to remote heterodyne detection of atmospheric pollutant gases. Application of this technique would permit single-ended, passive detection from both stationary and mobile sources. It is shown that, based on information obtained here on the SO_2 emission band at 8.7 μm, concentrations of the gas as low as 10 ppm can be detected, essentially independent of range, if the gas temperature is 100°C. For the same gas at 50°C, the minimum detectable concentration is about 50 ppm, and the measurements become more susceptible to changes in the background. Unfortunately, the present diode laser power capability is not sufficient to attain the ultimate remote heterodyne detection sensitivity, although progress is being made in both laser and detector technology.

Several other applications were studied during the first phase of this program.

1. Point Sampling. As has been demonstrated earlier, this technique using tunable lasers has the advantage of very high specificity by permitting testing at reduced pressure where overlap between adjacent absorption lines can be eliminated in most cases. With a 10-cm-long cell containing an NH_3 air mixture, and a tunable diode laser with 10 μW output power, the minimum detectable concentration was found

to be 28 ppm using a line having an absorption constant per unit pressure of 1 cm^{-1}/ Torr and an operating pressure of 4.5 Torr. For this test, second-derivative detection was used, which effectively enhances the desired signal.

2. "White" Cell Operation. Construction of a "white" cell permitted a path length of 7.3 meters to be used for point-sampling applications. Comparison of the signal-to-noise ratio using a 10-cm-long cell with that achieved by the "white" cell for identical gaseous concentrations showed the predicted enhancement; consequently, the minimum detectable concentration for the "white" cell is found to be about 0.3 ppm. Since these minimum detectable values are expected to be inversely related to laser power, it is clear that the use of tunable diode lasers in the milliwatt power range can yield much more sensitive point-sampling limits in the low ppb region.

3. Long-Path Transmission. Diode laser radiation was collimated with a lens and transmitted over a 75-meter path from one building to another. Although the experiment was preliminary, and no attempt was made to tune through any atmospheric SO_2 lines, a strong signal was received, indicating good potential for long-path transmission techniques using these devices.

4. Interferences. Some studies were made to find possible interferences between the spectral bands of certain other gases which may be found in the atmosphere and the 8.7-μm band of SO_2 by using the diode laser to scan portions of this band. Since NH_3 is used as the primary calibration standard for wavelength in this region, it can under certain conditions produce interference; however, there are only approximately 5 percent of the number of NH_3 lines as SO_2 lines in this region. A broader test was to place a quantity of automobile exhaust in the test cell, at 1 atmosphere pressure, and tune the diode laser over a region constituting strong SO_2 absorption. No interference was found, despite the many gaseous components in automobile exhaust.

DEVELOPMENT AND APPLICATION OF TUNABLE DIODE LASERS TO THE DETECTION AND QUANTITATIVE EVALUATION OF POLLUTANT GASES

1. INTRODUCTION

Tunable semiconductor diode lasers have been shown to have important potential application in remote or long-range sensing and point sampling of molecular pollutant gases.[1,2] Remote sensing can be accomplished by means of measurements of the infrared absorption or emission lines characteristic of a particular pollutant at atmospheric pressure. Point sampling permits gas pressures to be reduced until the Doppler-broadened infrared absorption structure is revealed, thereby making possible very high specificity. Since one measurement technique is used for all the pollutant gases, operational requirements are simplified. Moreover, the essentially instantaneous response is advantageous for a number of applications.

TABLE I
SELECTED WAVELENGTHS
FOR DETECTING ATMOSPHERIC POLLUTANT GASES

H_xC_y	3-4 μm	CH_2O	8.7 μm
CO	4.6	PAN*	8.7
NO	5.2	O_3	9.5
C_3H_8	6.8	C_2H_4	10.5
CH_4	7.7	NH_3	10.5
N_2O	7.7	C_3H_6	11.0
H_2S	7.8	C_2H_4O	11.5
NO_2	7.9	C_2H_6	12.0
SO_2	8.7	CO_2	13.9

* Peroxyacetyl nitrate.

Infrared spectroscopy is considered an important technique since each of the major molecular pollutants contains at least one strong band in the 3- to 15-μm "fingerprint" region of the infrared, as indicated in Table I. Dispersive infrared instruments now being used in the field usually have resolutions that are much poorer than the linewidths of typical gases at atmospheric pressure, and thus potentially useful information is lost. Even when high-quality spectrometers are used, the resolving power must be reduced so that a useful signal-to-noise ratio can be maintained with the relatively low power per unit spectral range available from incoherent sources. The use of gas lasers as nondispersive instruments, on the other hand, is restricted by the fact that these lasers cannot be tuned appreciably from their nominal wavelengths, and the match to pollutant gas absorption lines is seldom ideal.[3]

This program is concerned with the development of tunable semiconductor diode lasers and their potential application toward solving some of the air pollution monitoring problems. In Fig. 1-1 are shown wavelengths over which semiconductor lasers can be tuned by compositional

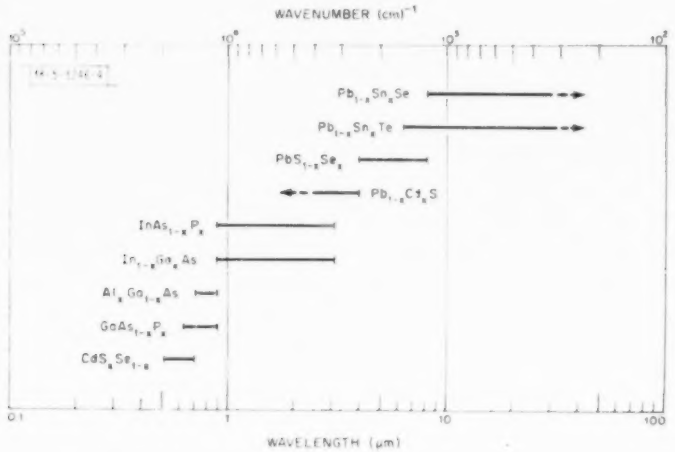

Fig. 1-1. Wavelength ranges which can be covered with alloyed semiconductor lasers. The arrows indicate possible further extension beyond present limits.

variations, from 0.5 μm in the visible to 32 μm in the infrared. It should be noted that it is possible to cover the entire 3- to 15-μm region of interest for monitoring gaseous pollutants with three semiconductor materials: PbCdS, PbSSe, and PbSnTe.

During the past year, PbSnTe diode lasers were developed for the 8.7-μm region in order to perform ultra-high-resolution spectroscopy on SO_2. Prior to this, PbSnTe lasers had been developed for operation in the 10-μm region, and had been used to study the spectral properties of ethylene (C_2H_4), ammonia (NH_3), and sulfur hexafluoride (SF_6), and to demonstrate the specificity, sensitivity, and reproducibility of point-sampling techniques using these lasers.[1] More recently, advances have been made in the development of tunable semiconductor lasers in new wavelength regions for the detection of other pollutant gases: for example, PbSSe at 4.6 μm for carbon monoxide (CO) detection[4] and at 5.2 μm for nitric oxide (NO) detection,[5] and PbCdS at 3.4 μm for detection of the C-H bond present in all hydrocarbons.[2] These advances were not made under EPA-sponsored programs, but are mentioned for completeness with regard to the current state of the art. The tunable diode lasers developed under this program are described in Section 2.

Section 3 contains some of the spectroscopic information obtained from the laser scans of portions of the ν_1 band of SO_2 between 1100 and 1200 cm^{-1}, with special attention to comparison between experiment and theory. Some of the actual laser scans are shown in Appendix A. In Appendix B are tabulated the line positions and strengths on the basis of these scans, as well as their identification from theory. Appendix C lists the NH_3 lines used for calibration. Section 3 in the main body of this report describes the linewidth and pressure-broadening studies as well.

Initial experiments confirming the theory for remote heterodyne detection are described in Section 4, and spectral emission lines from heated C_2H_4 were detected by this technique. At the present time, infrared laser and detector technology does not permit optimum use of this technique; however, calculations are presented which show the minimum detectable concentrations of various pollutant gases which might be measured by remote heterodyne detection after the state of the art has been suitably advanced.

Section 5 consists of experiments related to potential monitoring applications involving tunable lasers. The use of first and second derivative techniques in point-sampling applications is compared, and an experiment showing present limits of detectability is described. Preliminary studies of interference effects, temperature and pressure effects, and long-path transmission of diode laser radiation are also included in this section.

Appendices A, B, and C contain the actual SO_2 spectra, line tabulation, and NH_3 calibration line tabulation, respectively, as mentioned above. Appendix D contains a journal article published during the past year, and describing general applications of tunable diode lasers to air pollution monitoring. Appendix E contains an article submitted for publication, which essentially summarizes the laser spectroscopic measurements on SO_2.

2. DIODE LASER FABRICATION

In order to investigate the Doppler-limited high-resolution infrared absorption of the ν_1 band of SO_2 between 1100 and 1200 cm^{-1} (centered around 8.7 μm), $Pb_{1-x}Sn_xTe$ single crystals of the proper chemical composition (see Fig. 2-1) had to be prepared. Although tunable $Pb_{0.88}Sn_{0.12}Te$ diode lasers had been used for spectroscopic measurements of NH_3, C_2H_4, SF_6, and PF_5 in the 10-μm region, modifications in the crystal growth[6] and laser fabrication techniques were needed for those tailored to the 8.7-μm region.

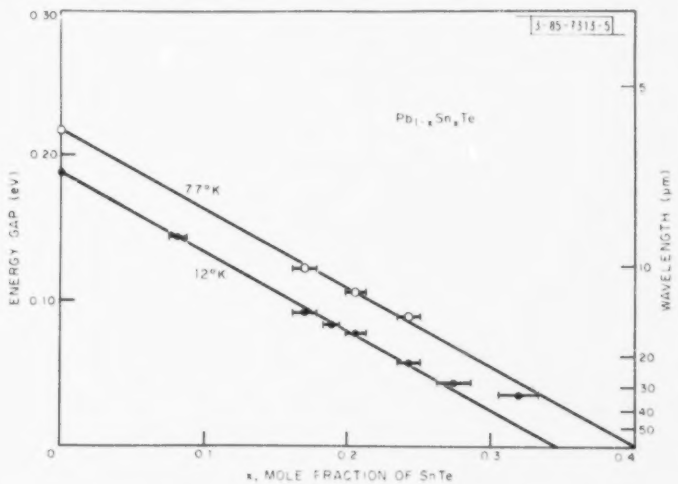

Fig. 2-1. Variation of $Pb_{1-x}Sn_xTe$ energy gap with mole fraction of SnTe at 12°K and 77°K.

In order to develop the new fabrication procedures, several crystals of $Pb_{1-x}Sn_xTe$ were grown from the vapor phase by two techniques: (1) a closed-tube vertical process, and (2) a recently developed closed-tube horizontal process. In each case the source consisted of a metal-rich, two-phase ingot of $(Pb_{1-x}Sn_x)_{1-y}Te_y$, with $y \approx 0.49$. Using a crystal growth temperature of approximately 800°C, most of the as-grown and air-cooled crystals were found to be n-type at room temperature for $x \gtrsim 0.08$, and p-type for $x \lesssim 0.08$. For $0.08 \lesssim x \lesssim 0.20$, an n-type surface layer is formed during the air-cooling process, producing p-n junctions for diode lasers operating in the 9- to 16-μm range. In order to obtain lasers for the SO_2 absorption measurements around 8.7 μm, x is approximately 0.07. Using the above procedure, the as-grown crystals are n-type with carrier concentrations of about 10^{18} cm^{-3}.

The best $Pb_{0.88}Sn_{0.12}Te$ diode lasers in the 10-μm region were made from crystals which were vapor-grown, annealed, and diffused (p-n junction formation) without ever having to open the growth ampoule. It is believed that elimination of the handling of these crystals by this procedure maintains the cleanest natural crystal surfaces possible, and is largely responsible for their superior performance over diodes prepared by conventional techniques. This procedure requires that the as-grown crystals are p-type, which, as mentioned above, is not the case for those where $x \approx 0.07$, where the solidus field shifts toward the metal-rich side of stoichiometry. In order to counter this effect, thallium metal was added to the two-phase ingot serving as the source for the vapor responsible for the crystal growth. (Thallium is a p-type impurity in PbSnTe, and therefore serves to compensate the donors produced by the shift in the solidus field.) In the vicinity of the p-n crossover temperature, the donor or defect concentration for metal-saturated crystals increases as temperature decreases. Consequently, by carefully controlling the thallium concentration it is possible to grow crystals, for which $x \approx 0.07$, at 800°C having p-type bulk conductivity, with an n-type skin formed on cooling.

Table II lists properties of the continuous-wave (CW), current-tunable PbSnTe diode lasers developed and used during the first year of this program. Some of these devices were continuously tunable over more than 1 cm^{-1} and produced some of the widest SO_2 scans shown in Appendix A. The single-mode output power from these devices is not yet sufficient for optimum heterodyne detection, as discussed in Section 4; the crystal growth parameters and laser fabrication techniques are being systematically studied in order to increase substantially the output power, so that heterodyne experiments using these lasers as tunable local oscillators will be feasible.

TABLE II

PROPERTIES OF CW $Pb_{1-x}Sn_xTe$ DIODE LASERS AT 10°K

Diode	x	Threshold Current Density (A/cm^2)	Maximum CW Output Power (μW) at I (amps)	Wavenumber at Threshold (cm^{-1})
284	0.0700	360 (1.05 A)	20 (2.2 A)	1142
286	0.0700	400 (0.75 A)	22 (2.0 A)	1160
301	0.0700	490 (0.91 A)	6 (2.0 A)	1128
302	0.0700	495 (0.91 A)	21 (2.0 A)	1132
315	0.0700	714 (1.52 A)	44 (2.4 A)	1150
317	0.0700	930 (1.80 A)	44 (2.0 A)	1148
326	0.0575	332 (0.60 A)	16 (0.9 A)	1179
328	0.0575	211 (0.34 A)	4 (2.0 A)	1200
329	0.0575	162 (0.23 A)	18 (0.8 A)	1206
338	0.0745	241 (0.60 A)	12 (1.0 A)	1104

3. LASER SPECTROSCOPY OF SULFUR DIOXIDE

Three major absorption bands of SO_2 in the 2- to 15-μm region are shown in the grating spectrometer scans of Fig. 3-1, adapted from Pierson, Fletcher, and St. Clair Gantz.[7] Centered at 8.7 μm is the ν_1 vibration-rotation band, at 7.3 μm is the ν_3 band, and at 4 μm is the $\nu_1 + \nu_3$ combination band. At the start of this program there were no tunable semiconductor lasers in the 4 μm region. Such devices have since been developed by Nill, Blum, Calawa, and Harman,[4] and by Melngailis and Harman.[8] Although the ν_3 band is somewhat stronger than the ν_1 band, it is in a region of strong water vapor absorption, which may produce interference effects during atmospheric transmission over long paths. A secondary reason for selecting the longer wavelength is that it provides greater sensitivity for remote heterodyne detection, as will be illustrated in Section 4.

Figure 3-2 is a grating spectrometer scan of the ν_1, 8.7-μm band of SO_2, as recorded by Shelton, Nielsen, and Fletcher;[9] it represents most of the 1100- to 1200-cm^{-1} region of interest for the present study. There are several thousand lines in this band which overlap in varying

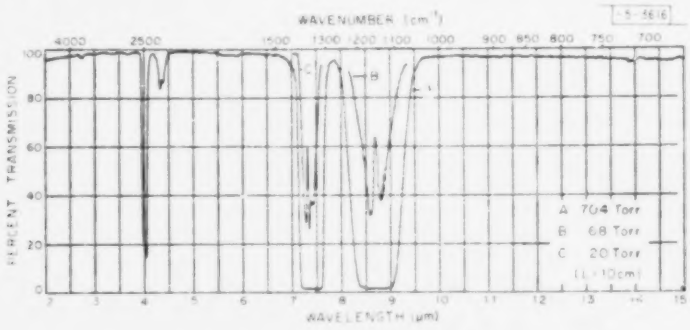

Fig. 3-1. Grating spectrometer scan of SO_2 absorption at room temperature, between 2 and 15 μm, from Pierson, Fletcher, and St. Clair Gantz.[7] The curves labeled A, B, and C represent gas pressures of 704, 68, and 20 Torr, and slit-width settings of 0.927, 0.900, and 0.900 mm, respectively, for the Perkin-Elmer Model 21 infrared spectrophotometer used. Cell length (L) is 10 cm.

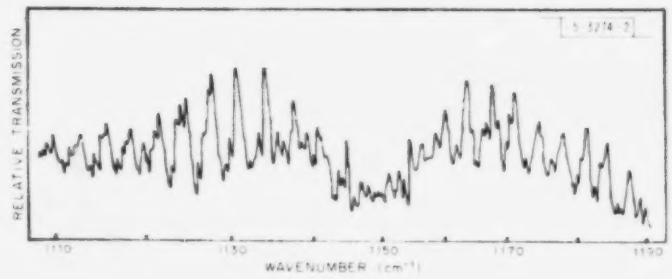

Fig. 3-2. Grating spectrometer scan of the ν_1 vibration-rotation band of SO_2 at room temperature, after Shelton, Nielsen, and Fletcher.[9] Effective path length (L) is 20 meters, and instrumental resolution 0.3 cm^{-1}. Although not explicitly stated by the authors, SO_2 pressure appears to be approximately 1 Torr.

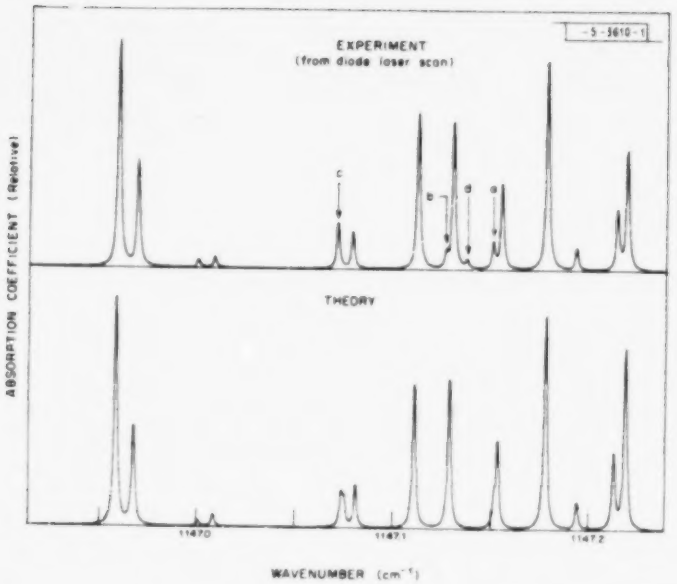

Fig. 3-3. Comparison between measured and calculated absorption coefficients and positions for some lines in the ν_1 band of SO_2. These scans were computer-generated using Lorentzian profiles. Lines designated as a, b, and c represent the transitions (29,6,24)←(28,7,21), (35,7,29)←(34,8,26), and (26,4,22)←(27,3,25), respectively. Line d is not predicted by the present theoretical model.

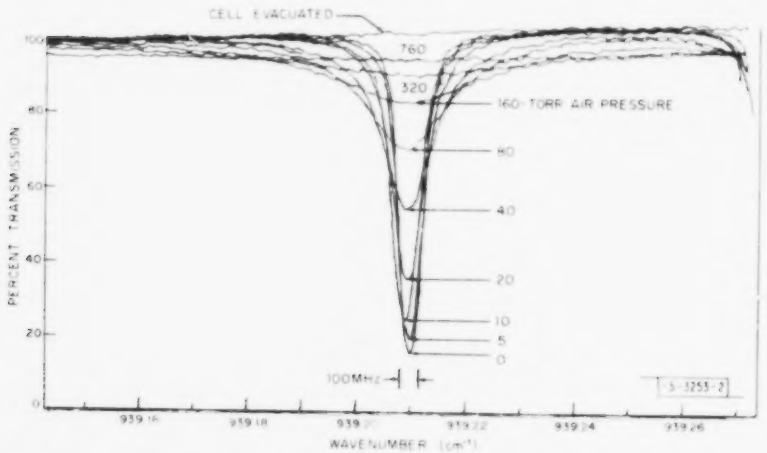

Fig. 3-4. Absorption line profile of aQ(9,3) line of NH_3, at 2 Torr pressure, with different partial pressures of air, from zero to 1 atmosphere (760 Torr). L = 30 cm, T = 296°K (23°C).

degrees at atmospheric pressure to produce a spectrum quite similar to that of Fig. 3-2 (limited by the resolution of the spectrometer). These lines can be revealed individually at reduced pressure using the ultra-high-resolution capability of tunable semiconductor diode lasers, with demonstrated linewidths of $3 \times 10^{-6}\,cm^{-1}$ or less.[10]

The SO_2 was obtained from the Matheson Company, Inc. of East Rutherford, New Jersey, and had a quoted purity of 99.98 percent. Using the tunable PbSnTe lasers described in Section 2, several hundred of the SO_2 absorption lines were measured in various segments of the ν_1 band. Wavelength calibration was obtained by placing NH_3 in the cell after each SO_2 scan. The NH_3 lines have been precisely measured[11] and are normally used as wavelength calibration standards in this region of the infrared. The length of the gas cell was 30 cm, and a spectrometer using a Ge:Cu detector was used for approximate determination of laser wavelength and to limit the detected signal to a single laser mode. Some of the actual laser scans are shown in Appendix A, and in Appendix B the fundamental absorption constants (per unit pressure) of these lines are tabulated. For reference, the NH_3 calibration lines used are listed in Appendix C.

A theoretical spectrum for the ν_1 band of SO_2 has been calculated by S. A. Clough[12] using the method described in Ref. 13 based on accurate microwave values[14] of the rotation constants for both the ground and first excited state of this vibration-rotation mode. When the experimental and theoretical values for the absorption constants are compared, as in Fig. 3-3 for the $1147\text{-}cm^{-1}$ region, the SO_2 transitions can be identified. For example, the large absorption line at $1146.966\,cm^{-1}$ is produced by the transition (14,1,13)←(14,2,12), where the three quantum numbers are (J, K_A, K_C). On the basis of these experiments, the value of the frequency of the ν_1 band center was found to be $1151.71\,cm^{-1} \pm 0.01\,cm^{-1}$, which can be compared with the experimental value previously measured of $1151.38\,cm^{-1}$ (Ref. 9). Lines a, b, and c are shifted slightly from their predicted positions, and are described more fully in Appendix E. All the lines predicted by theory have been observed experimentally; however, a few lines which have been observed are not predicted, such as line d in Fig. 3-3, which may represent a "hot" band of SO_2 (involving the first excited vibrational state of the bending (ν_2) mode, which was not included in the theory), another isotope, or a weaker transition not included in the theory. There is always the chance that these extraneous lines may represent impurities in the SO_2, but their infrequent occurrence makes them relatively unimportant at present.

The above theoretical model for the ν_1 band of SO_2 now permits us to predict the structure of either absorption or emission spectra under any conditions of gas temperature, pressure, or instrumental resolution. This knowledge is essential for any spectroscopic technique of monitoring SO_2, and is presently being used to determine the optimum wavelength for detection by infrared absorption at atmospheric pressure and elevated temperatures. A similar theoretical model has already been established for ozone (O_3) in the 9.5-μm region;[15] ultimately, it would be very useful to have a complete theoretical model of a polluted atmosphere.

The rates of pressure broadening of the SO_2 lines were measured and compared with those for NH_3 in the 10-μm region. The effect of increased air pressure on the shape of an NH_3 absorption line is shown in Fig. 3-4, with the corresponding effect on the absorption coefficient illustrated by Fig. 3-5 for both NH_3:air (where the absorption coefficient decreases linearly with increasing pressure above about 10 Torr) and NH_3:NH_3 (where the absorption coefficient reaches a steady value in the pressure-broadened regime). The spectral lines were fitted with

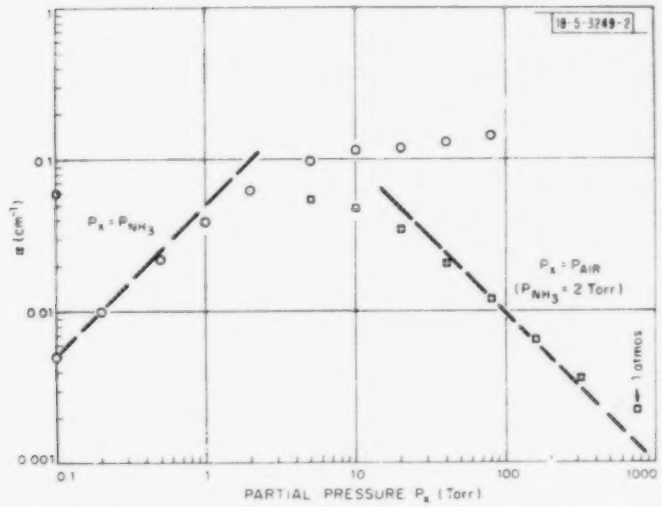

Fig. 3-5. Pressure dependence of absorption coefficient of aQ(9,3) NH_3 line for both self- and air-broadening.

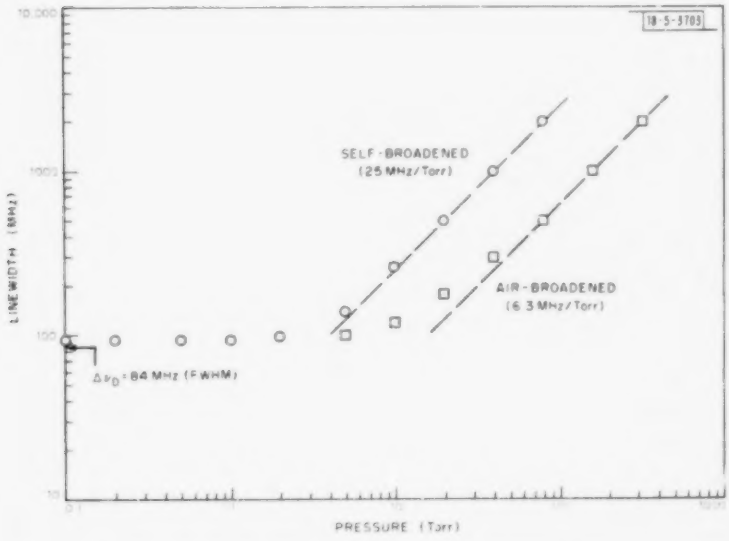

Fig. 3-6. Collision-broadening of full linewidth at half-maximum intensity (FWHM) for aQ(9,3) NH_3 line centered at 939.21 cm^{-1}, for both self- and air-broadening. Theoretical Doppler-limited linewidth (FWHM) is 84 MHz (0.0028 cm^{-1}) at 296°K.

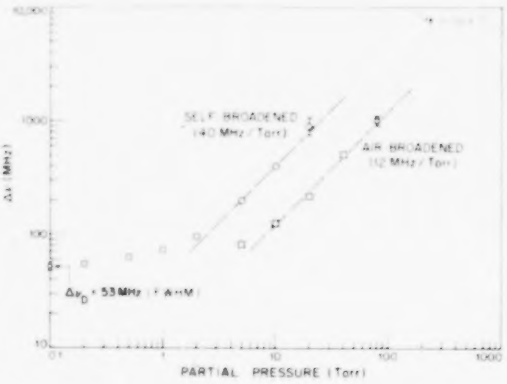

Fig. 3-7. Collision-broadening (FWHM) of two SO_2 lines at 296°K: $(15,4,12)\leftarrow(15,3,13)$ at 1163.297 cm^{-1}, and $(8,0,8)\leftarrow(8,1,7)$ at 1148.810 cm^{-1}. Doppler-limited linewidth (FWHM) is 53 MHz (0.0018 cm^{-1}).

theoretical Lorentzian and Gaussian curves (where appropriate) in order to accurately determine the effective linewidths at the various pressures. The full linewidth at half-maximum intensity (FWHM) for NH_3 is shown in Fig. 3-6, and for SO_2 in Fig. 3-7. With air-broadened FWHM values of 6.3 and 12 MHz/Torr for NH_3 and SO_2, their respective linewidths at atmospheric pressure are 0.16 cm^{-1} and 0.30 cm^{-1}. Some workers refer to the half-width at half-maximum intensity (HWHM), which would be 0.08 cm^{-1} and 0.15 cm^{-1} at atmospheric pressure for NH_3 and SO_2, respectively.

4. REMOTE HETERODYNE DETECTION

Heterodyne detection of characteristic infrared emission from atmospheric pollutant gases may represent the ultimate remote-sensing technique for source monitoring. Its operation is monostatic (single-ended), passive, and essentially range-invariant. Heterodyne detection involves the same emission lines monitored by passive incoherent infrared systems, but without restrictions such as loss of resolution due to instrumental broadening of the lines (reduced specificity) and non-ideal detector-noise-limited operation (reduced sensitivity). Some coincidences between fixed-frequency gas laser wavelengths and those of atmospheric-pressure-broadened pollutant emission lines suggest their application as local oscillators (L.O.) in the heterodyne scheme.[16] It is clear, however, that the ability to "tune" the L.O. wavelength ideally to the center of the emission line as well as to a region where there is no characteristic radiation is important for the elimination of background effects, and thus provides better ultimate sensitivity. Fixed-frequency infrared gas lasers cannot normally be tuned more than the 50- to 100-MHz ($1.8 - 3.6 \times 10^{-3}$ cm^{-1}) Doppler width, whereas the required shift for gases in the atmosphere is at least 10,000 MHz (0.33 cm^{-1}), which can easily be achieved with tunable semiconductor diode lasers.

Calculations were made of the sensitivity limits for remote heterodyne detection of several important pollutant gases at different temperatures. The instrumentation, theoretical analysis, and numerical predictions are contained in Section 4.1. Quantitative experimental verification of the basic heterodyne theory has been achieved for radiation from a thermal source (analogous to an optically thick gas at line center) and is described in Section 4.2.

At the present time, tunable diode lasers, even with single mode power levels of tens of milliwatts, cannot provide sufficient L.O. power for optimum heterodyne detection using

state-of-the-art low-noise amplifiers and infrared detectors. In Section 4.3 this will be discussed in detail. In order to circumvent the tunable L.O. problem temporarily and permit the detection of actual emission lines from a heated gas, a fixed-frequency CO_2 laser was used as the L.O. in an experiment to detect heated ethylene (C_2H_4) gas at low pressure. Although a tunable L.O. is usually necessary to obtain spectral information, electronic scanning of the wideband (500-MHz detector/amplifier) signal with a narrowband (34-MHz) filter simulated the ultimate system. This experiment is described in Section 4.4.

4.1 Heterodyne Theory and Calculations

Figure 4-1 illustrates schematically the operation of remote heterodyne detection. The telescope receiving optics collects characteristic radiation from the gases in the stack plume and images it onto the infrared detector. By means of a beam splitter, tunable laser radiation also impinges on the detector, and power at the difference (heterodyne) frequency is measured electronically. If the solid angle subtended by the source at the detector is larger than the diffraction-limited solid angular resolution of the collection optics – a situation usually valid for smokestack plumes at ranges up to 1 km and with collection optics as small as 1 cm^2 – the signal-to-noise voltage ratio (after square-law detection) is given by[1]

$$S/N = \xi\eta\left(1 - e^{-\alpha'_c cL}\right)\left(\frac{1}{e^{h\nu/kT_s} - 1} - \frac{\epsilon_b}{e^{h\nu/kT_b} - 1}\right)\sqrt{B\tau} \quad , \tag{4-1}$$

where ξ represents the fraction of emission energy absorbed by the detector, η is the detector quantum efficiency, α'_c is the absorption constant of the particular spectral line per ppm, c is the actual concentration in ppm, B is the intermediate-frequency (IF) bandwidth of the detection system, τ the post-detection integration time, $h\nu$ the infrared photon energy, L the thickness of the plume and T_s its temperature, and ϵ_b is the emissivity of the background at temperature T_b. The following assumptions have been made: (a) that the IF bandwidth is less than the emission linewidth; (b) that the emission and absorption due to the pollutant in the ambient atmosphere are not important because of its low concentration in the atmosphere relative to that in the plume; (c) that the background attenuation from the wings of other molecular absorption lines is negligible; (d) that the local oscillator has sufficient power to overcome the other sources of noise (this will be discussed in detail in Section 4.3); and (e) that a photovoltaic detector is being used. (If a photoconductive detector is used, S/N is reduced by a factor of two.)

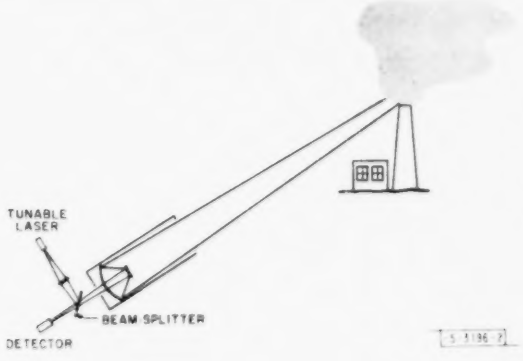

Fig. 4-1. Configuration for remote, single-ended, heterodyne detection of pollutant gases from emission sources.

Since ϵ_b is often much smaller than unity (about 0.1 in the 10-μm region of the infrared when there are no clouds in the background), the source does not have to be hotter than the background; in fact, it could be colder, as will be demonstrated. Using Eq. (4-1) for the pollutant concentration c in ppm, we obtain the following expression:

$$c = -\frac{1}{\alpha_c' L} \ln\left[1 - \frac{(S/N)}{\xi\eta\zeta(B\tau)^{1/2}}\left(1 + P_{LO}^{o}/P_{LO}\right)\right] \quad . \tag{4-2}$$

where ζ is the bracketed Bose-Einstein term in Eq. (4-1), P_{LO} is the L.O. power, P_{LO}^{o} is the L.O. power required to generate noise in the detector which just equals that produced by other sources [in assumption (d) above, the L.O. power swamped the other noise contributions]. If we further assume that $P_{LO} = P_{LO}^{o}$, that S/N = 4, and that $\eta = \xi = 1$ (corresponding to an ideal photovoltaic detector and efficient collection optics), the above equation reduces to

$$c = -\frac{1}{\alpha_c' L} \ln\left[1 - \frac{8}{\zeta(B\tau)^{1/2}}\right] \quad . \tag{4-3}$$

Diode laser scans of the spectral lines of CO, NO, NH_3, C_2H_4, and SF_6 indicate approximately equal strengths for the strongest lines of these gases of $\alpha_c' = 10^{-5}\ \mathrm{cm}^{-1}/\mathrm{ppm}$ at atmospheric pressure. (The effective strength of SO_2 at 8.8 μm is an order of magnitude smaller.) If we let B = 500 MHz, τ = 10 sec, L = 10 meters (reasonable for a power-plant stack diameter), T_b = 293°K, and ϵ_b = 0.2, the minimum detectable concentrations at different temperatures are those shown in Fig. 4-2 as a function of wavelength. Note that sensitivity is greater at longer

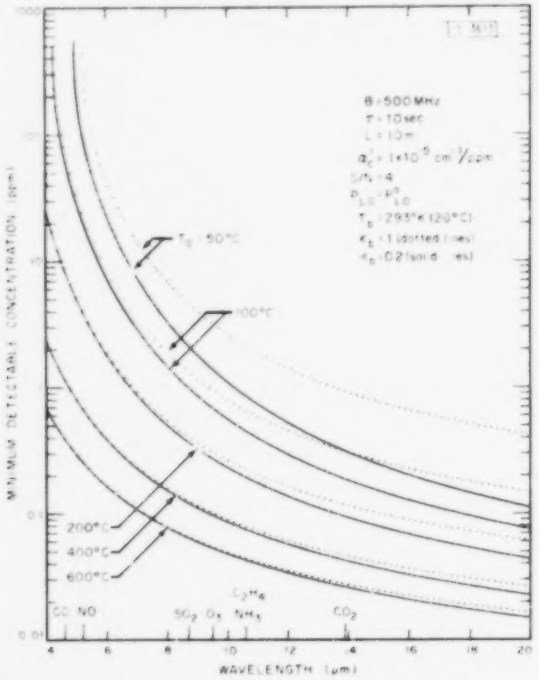

Fig. 4-2. Calculated wavelength dependence for pollutant monitoring using the heterodyne technique, for various gas temperatures, and background emissivities of 0.2 and 1.0. Useful wavelengths for some pollutant gases are indicated on the abscissa. Other parameters are indicated in the figure.

wavelengths, which is a major consideration to be made in selecting optimum emission lines for heterodyne detection. Note also that, even at temperatures as low as 50°C, 2 ppm of C_2H_4 and NH_3 can be detected at 10.6 μm. The wavelength dependence of sensitivity is particularly noticeable at low gas temperatures. For example, for a gas at 50°C it will not be possible to obtain any useful sensitivity with this technique at wavelengths shorter than 5 μm; however, at higher temperatures, even CO and NO in the effluent of stationary or mobile sources can be detected adequately.

Although SO_2 emits strongly around 4 μm, in addition to the 8.8-μm band indicated in Fig. 4-2, the sensitivity (for lines of equal strength) at the latter wavelength is one or two orders of magnitude better, depending on the gas temperature. In order to determine the sensitivity for remote heterodyne detection of SO_2 in the 8.8-μm region, we use the parameters assumed above, but substitute the proper value of $\alpha_c' = 10^{-6}$ cm^{-1}/ppm which we have measured for SO_2 at atmospheric pressure. The theoretical curves of Fig. 4-3 illustrate how the ultimate sensitivity depends on temperature and background emissivity. An increase in the L.O. power beyond the value P_{LO}^o produces at best, in accordance with Eq. 4-2, only a factor-of-two improvement in ultimate sensitivity. (This is one reason why $P_{LO} = P_{LO}^o$ is a good design parameter to use.) It should also be noted that the minimum detectable concentration ranges from 2 to 50 ppm for SO_2 gas temperatures from 300 to 50°C, respectively.

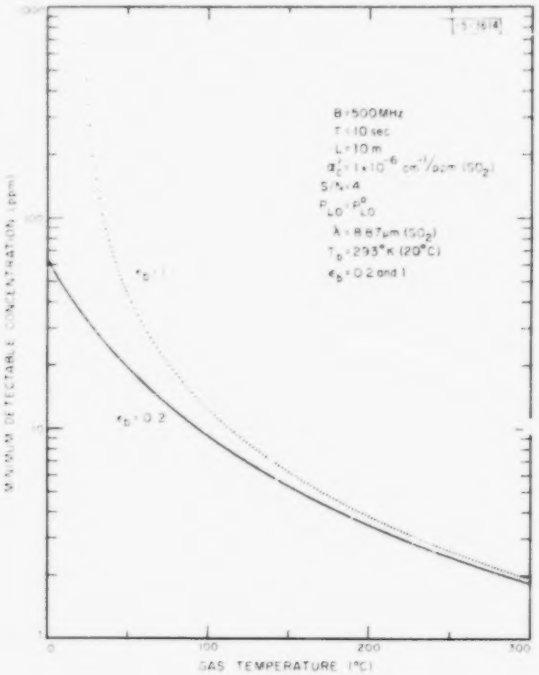

Fig. 4-3. Theoretical temperature dependence for heterodyne detection of SO_2, for a signal-to-(rms)-noise ratio of 4, and background emissivities of 0.2 and 1.0. Other parameters are indicated in the figure.

4.2 Heterodyne Detection of Thermal Radiation – Test of Theory

In order to show G-R noise-limited operation,[17] the experimental setup of Fig. 4-4 was used, which involved heterodyne detection of infrared radiation in the 10-μm region from a globar at about 1500°C (1773°K), using a CO_2 laser as fixed-frequency local oscillator.

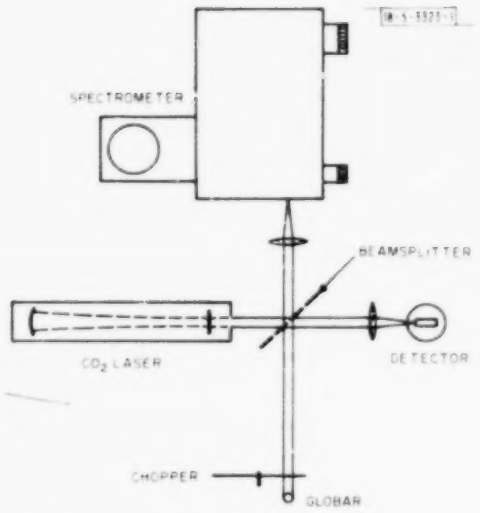

Fig. 4-4. Experimental setup for in-laboratory detection of thermal radiation using the infrared heterodyne technique. The lenses are BaF_2, and the beam-splitter is coated Irtran IV.

Fig. 4-5. Heterodyne signal between CO_2 laser and thermal source at a temperature of 1500°C. System bandwidth is 450 MHz, and post-detection integration time 0.1 sec. Origin of the time axis is arbitrary.

Realizing that gas emission lines at atmospheric pressure are several GHz wide (~5 GHz for NH_3 at 10 μm, ~9 GHz for SO_2 at 8.8 μm), it is important to use the widest IF bandwidth possible consistent with a low amplifier noise figure and the frequency limitations of the infrared detector. At present, 450 MHz is the best value, with available amplifiers having noise figures in the 2.4- to 4.0-dB range. This experiment was performed with an amplifier having an average noise figure of 4.0 dB over 450 MHz, yielding an equivalent noise temperature of T_A = 438°K. At the 10.6-μm wavelength of the CO_2 laser, $h\nu/e$ = 0.12 V. The infrared detector is a liquid-helium-cooled Ge:Cu photoconductor, with η = 0.5 and a gain G of 0.07 at an applied bias of 22.5 V. The load resistance R_L was 25 ohms.

In Fig. 4-5 is shown an actual recorder trace of the heterodyne signal between the globar source and the CO_2 laser, for which the local oscillator power is greater than that needed to overcome amplifier noise. The signal vanishes when either the CO_2 laser or the globar is blocked, and in the latter case the observed G-R noise is within a factor of two of the predicted value for the 40-mA detector L. O. current. When the laser itself is blocked, the small residual noise is produced by the amplifier. Since the G-R noise has overcome the amplifier noise, the ultimate heterodyne signal-to-noise is being achieved, subject to optical transmission losses and other losses present in the globar light path and other factors to be discussed later.

Quantitative verification of Eq. (4-1) was obtained by replacing the globar with a calibrated 600°C thermal source and comparing the predicted and observed signal-to-noise ratio. Using a 2.4-dB (noise-figure) amplifier and a detector bias of 40 V, G-R noise-limited operation was again established. The transmission of the Irtran II beam splitter (0.5), BaF_2 lens (0.85),

BaF_2 dewar window (0.85), and detector front surface (0.64) produced a value for the transmission factor ξ of 0.23. If we let T_s = 872° K (600° C), T_b = 292° K (20° C), ϵ_b = 1, B = 450 MHz, and τ = 0.3 sec, Eq. (4-1) becomes

$$\frac{S}{N} = \frac{(0.23)\,(0.5)}{2}\,(0.292 - 0.012)\,\sqrt{450 \times 10^6 \times 0.3} = 187 \quad .$$

The measured ratio of signal voltage to rms noise voltage (output voltage is proportional to input power because of the rf detector) is 52, implying a mixing efficiency of 28 percent. (By comparison, we have observed heterodyne mixing efficiencies of 12 percent for gas laser/diode laser experiments, and as high as 75 percent for diode laser/diode laser beating experiments, so that the result appears to show reasonably good agreement with theory.) It should ultimately be possible to approach 100 percent efficiency by proper optical phase matching.

There are several steps which can be taken to enhance the signal-to-noise ratio from its predicted value of 187 for the above experiment. Such improvement centers on reducing the optical transmission losses and use of a different type of infrared detector. This will be discussed in Section 4.3.

Since reasonable agreement between theory and experiment was obtained for both the noise voltage and the signal-to-noise ratio at a fixed temperature, it remained to verify the temperature dependence of Eq. (4-1). Since P_N is not a function of the source temperature T_s, there should be a linear dependence between the square-law-detected signal voltage (proportional to P_s) and the bracketed term γ, defined earlier. This dependence is followed, as shown in Fig. 4-6 for source temperatures between 700 and 1200°K (428 to 928°C). Although not shown here, heterodyne detection was observed for source temperatures as low as 200°C using a 4-dB (N. F.) amplifier.

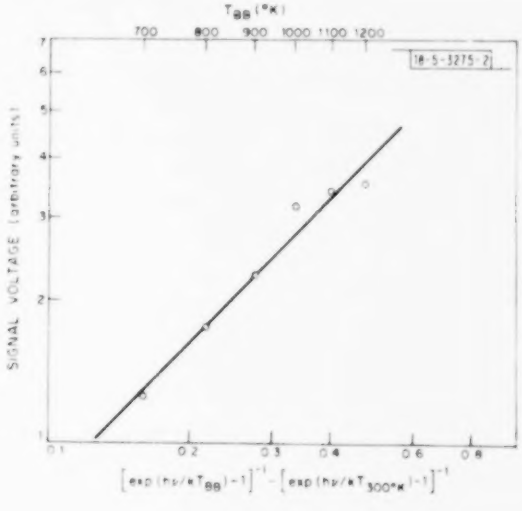

Fig. 4-6. Heterodyne signal voltage as a function of Planck function for several source temperatures from 700 to 1200°K (973-1473°C). CO_2 laser wavelength is 10.64 μm, and system bandwidth is 450 MHz.

4.3 Local Oscillator Power Requirement

The local oscillator power necessary to produce a noise level equal to that of the preamplifier is defined as follows [17]

$$P_{LO}^{o} = \frac{(kT_A/e)(h\nu/e)}{\eta G^2 R_L} \quad . \tag{4-4}$$

where T_A is the noise temperature of the amplifier, G the infrared detector gain, R_L the load resistance, and e the electronic charge. For a 2.4-dB amplifier (T_A = 240°K), η = 0.5, G = 0.12, R_L = 50 ohms, and $\lambda = c/\nu = 10\,\mu m$,

$$P_{LO}^{o} = \frac{(0.018)(0.12)}{(0.5)(0.12)^2(25)}\ W = 12\,mW \quad .$$

This calculation illustrates why the $Pb_{1-x}Sn_xTe$ diode laser power (we have measured 1 mW in a single laser mode for the best case) is not yet sufficient to achieve ultimate sensitivity in remote heterodyne detection using present amplifiers and infrared detectors.

In heterodyne detection the L.O. power can, in principle, be increased sufficiently for G-R noise to swamp other noise components. Consequently, infrared detectors with very high detectivities are not required, and there can be definite advantages to replacing the photoconductor with a photodiode. A photodiode does not sacrifice gain in order to obtain high frequency response, the gain, in fact, is usually assumed to be unity, and the quantum efficiency η characterizes the performance of the detector. Although presently available wideband photodiodes have quantum efficiencies of not more than 0.2, improvements are continually being made. If we assume η = 1, an inherent detector gain of unity, and neglect optical losses, Eq. (4-4) yields P_{LO}^{o} = 86 μW, which has been obtained in a single mode for tunable semiconductor diode lasers in this wavelength region. Thus, improvements in both areas of technology – higher tunable laser power and more efficient photodiodes – would advance the achievement of remote heterodyne detection.

4.4 Heterodyne Detection of Ethylene

In Fig. 4-7 is shown a heterodyne-calibrated absorption spectrum of SF_6 around the P(14) CO_2 laser line, as well as a similar scan of C_2H_4 at room temperature and 100 mTorr pressure. Within 450 MHz (the bandwidth of our system) of the P(14) line, there are two distinct C_2H_4 absorption lines. These become characteristic emission lines when focused onto a cold detector, as in Fig. 4-8, and the emitted signal increases according to Eq. (4-1) as the gas temperature is raised.

The experimental schematic of Fig. 4-9 was needed in order to obtain spectral information during the heterodyne detection experiment, since a fixed-frequency laser – not a tunable laser – was used as the local oscillator. The gas and laser beams are combined at the detector D. The load resistance R_o of 50 ohms terminates the line to the amplifier (reducing electrical reflections between detector and amplifier), and the capacitor C_o blocks the DC bias from this path. The signal is fed into a low-noise (2.5 dB), wideband (450 MHz) amplifier, then to a mixer for combination with a sweep generator signal (0 to 450 MHz). The narrowband amplifier at the output of the mixer passes only that electrical information within 17 MHz of the sweep generator frequency. This signal is then rectified by the RF detector into a steady voltage (except for the

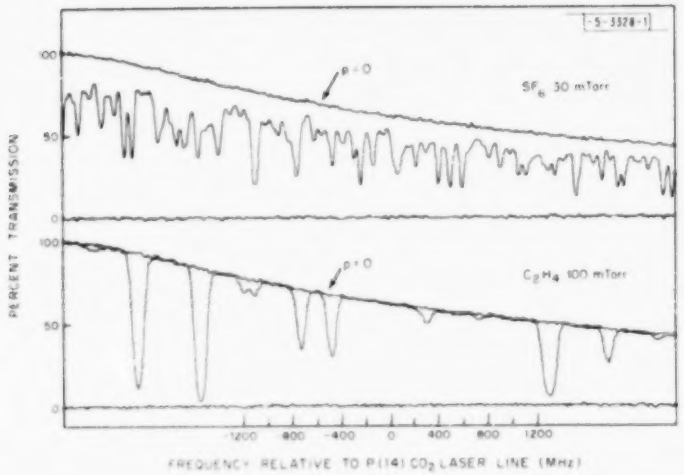

Fig. 4-7. Heterodyne-calibrated scan of SF_6 (upper) at 30 mTorr pressure, referenced to P(14) CO_2 laser line. The lower scan represents C_2H_4 at 100 mTorr pressure over the same tuning range. L = 30 cm, T = 296°K.

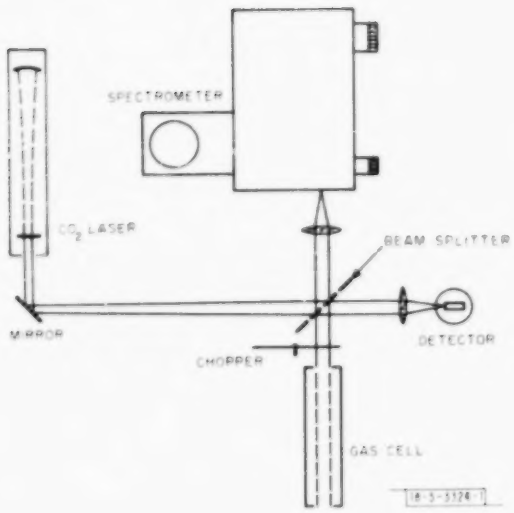

Fig. 4-8. Experimental configuration for heterodyne detection of infrared emission lines. Windows on the gas cell are made of BaF_2.

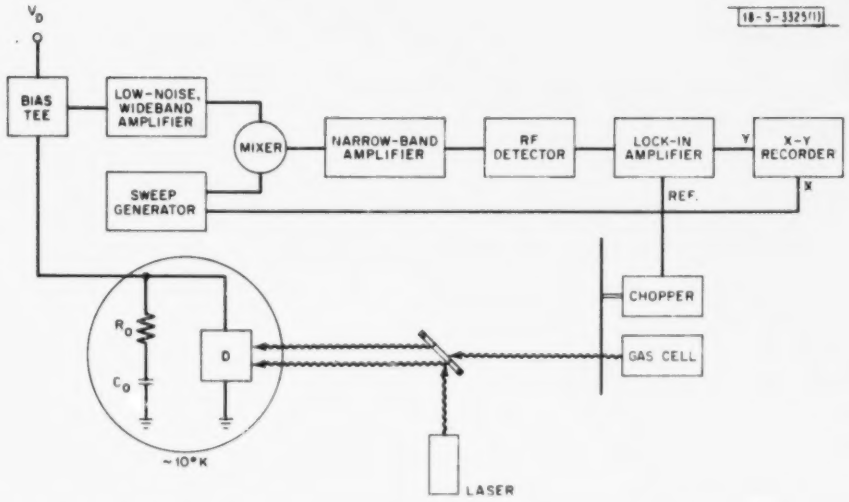

Fig. 4-9. Schematic for heterodyne emission spectroscopy with fixed-frequency laser local oscillator.

modulation caused by the mechanical chopper in the beam from the gas cell), and then synchronously detected by the lock-in amplifier and displayed on an X-Y recorder. The resulting signal is shown in Fig. 4-10 for C_2H_4 pressures of 0, 1, and 3 Torr at a temperature of 600°C in a 1-meter-long cell. Although the signal-to-noise ratios for these scans do not represent the ultimate values (caused in part by absorption by the C_2H_4 near the relatively cool cell window), and a time constant of 30 seconds was required, this experiment represents the first remote heterodyne detection of thermal emission lines. When improved infrared detectors in conjunction with stronger tunable lasers permit super-heterodyne techniques to be used, the narrow-band amplifier and mixer of Fig. 4-9 will become unnecessary, and further improvement in the signal-to-noise ratio by signal-averaging of repeated laser scans through the emission line will be possible.

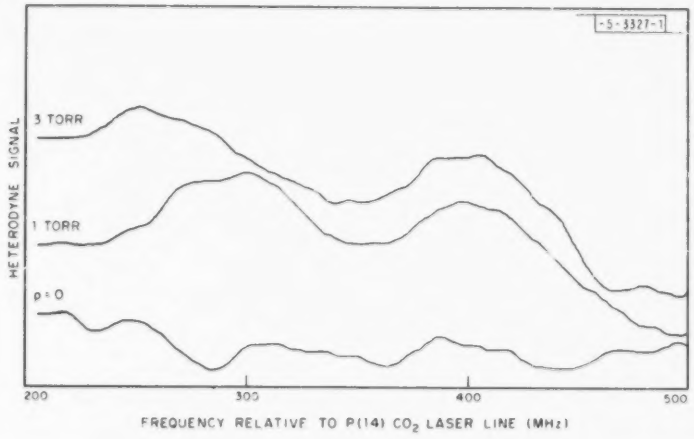

Fig. 4-10. Heterodyne detection of emission from C_2H_4 at 600°C, using the P(14) CO_2 laser line as fixed-frequency local oscillator. System bandwidth is 450 MHz, effective scanning bandwidth is 17 MHz. The only difference between curves is the indicated change in pressure of the gas.

5. EXPERIMENTS RELATED TO MONITORING APPLICATIONS OF TUNABLE LASERS

Several experiments were performed to provide some insight into the use of tunable lasers – particularly tunable diode lasers – in monitoring applications. In Section 5.1 a sensitivity measurement for point-sampling is described, involving a tunable diode laser and infrared detector. Section 5.2 considers effects produced on the SO_2 absorption spectrum by changes in gas temperature and increases in pressure to one atmosphere. In another experiment, no interference was produced by a sample of polluted air at atmospheric pressure for the wavelength range used. In Section 5.3 a long-path atmospheric transmission experiment of diode laser radiation is described.

5.1 Point Sampling Sensitivity Measurement

We have shown earlier[1] that in point-sampling applications it is possible to eliminate (in most cases) any interference effects between different gaseous components of a specimen to be analyzed by reducing the net gas pressure to the point where the characteristic absorption spectra are revealed and overlap caused by pressure-broadening is negligible. In the experiment to be described, the diode laser frequency was modulated at 500 Hz by a small (~1 mA) current superimposed on the steady diode current. When the diode laser emission scans an absorption line, a first derivative of the absorption line profile is produced if the synchronous amplifier is tuned to 500 Hz (this procedure was used in Ref. 1 to detect C_2H_4 in automobile exhaust). If a reference signal of 1 kHz is applied to the synchronous amplifier, and the amplifier set to that frequency, the second derivative of the absorption line profile is produced. Results of such an experiment, involving the detection of an NH_3 line of strength 1 cm^{-1}/Torr, are shown in Fig. 5-1. Trace A represents the second derivative signal produced in a 10-cm-long

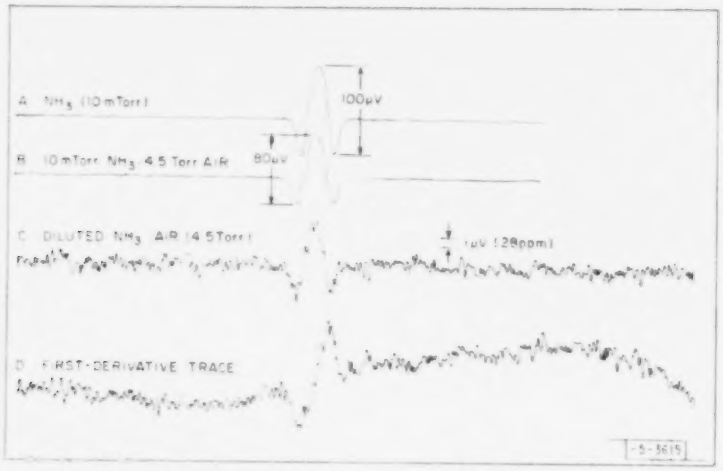

Fig. 5-1. Point-sampling sensitivity measurement using a 10-cm-long cell and Ge Cu infrared detector. (A) Second-derivative trace of NH_3 line at 10 mTorr pressure. (B) Second-derivative trace of the same line when 4.5 Torr air is added; (C) Second-derivative trace of (B) after sequential dilutions with air until the signal at 4.5-Torr pressure was comparable to the detector noise level, which represents approximately 28 ppm peak-to-peak. Curve (D) is a first-derivative trace of (C), illustrating long-term fluctuation effects not present in the second-derivative scans shown above.

absorption cell by NH_3 at 10-mTorr pressure; the peak-to-peak voltage is 100 μV. Trace B shows the effect produced by the addition of 4.5 Torr of air: slight broadening of the signal (see also Fig. 3-6) with corresponding reduction in signal to about 80 μV. In an attempt to determine the minimum detectable concentration of NH_3 using this point-sampling technique, several dilutions of the gas were made until Trace C was obtained, showing a peak-to-peak noise of approximately 1 μV. Since 80 μV represented a partial NH_3 pressure of 10 mTorr, and the signal is directly proportional to gas concentration in this region, 1 μV corresponds to 0.125 mTorr NH_3, or 28 ppm in 4.5 Torr of air. Since the noise level represents detector noise which is not caused by the laser, it is possible to increase sensitivity by using a laser having more than the 10-μW power of the device used for Fig. 5-1. (At some point, however, the detector noise would increase also, due to photon noise, as the square root of the laser power;[17] however, the signal would increase linearly, resulting in still better sensitivity, but at a slower rate of improvement.) Trace D is the first derivative signal, exhibiting nearly the same signal-to-noise as that of Trace C under the same conditions, but with the added complication of a slow change in signal strength over the width of the scan. This signal variation probably represents the change in laser power over this region.

Further improvement in point-sampling sensitivity can be obtained by increasing the path length with a multireflection "white" cell.[18] During the past year, a 'white" cell with an effective path length of 730 cm was constructed in accordance with the design suggestions of P. L. Hanst. The 8-pass unit consists of two spherical mirrors, each with a focal length of 45.7 cm, placed 91.4 cm apart. Two partial quadrants were removed from one of the mirrors to make room for the entrance and exit beams. The other mirror was cut into semicircular halves to permit beam direction within the cell. When the beam from a tunable diode laser was directed through the multipass cell, the first-derivative signal obtained by scanning through an NH_3 absorption line was 73 times greater than that obtained while scanning the same line using a 10-cm-long cell, as expected. Since the detector noise level remains the same, we conclude that the use of this "white" cell makes it possible to detect concentrations 73 times smaller than the noise level of Fig. 5-1 (28 ppm), or a few hundred ppb using a 10-μW diode laser.

5.2 Pressure, Temperature, and Interference Effects

In certain applications of infrared spectroscopy to pollutant monitoring, such as long-path absorption or emission in the atmosphere, it is not possible to control the experimental conditions as well as can be done in point sampling. The work of Burch, Pembrook, and Gryvnak, using a high-resolution grating spectrometer,[19] showed that for temperatures between 23°C and 300°C the net absorption strength of the ν_1 SO_2 band is constant, although there are changes in the relative strengths of individual lines within the band. They further show that the characteristic spectrum of SO_2 in the atmosphere is essentially independent of temperature in the 1127- and 1180-cm^{-1} regions of the ν_1 vibration-rotation band. A study was made of the temperature dependence of isolated lines at reduced (1-Torr) pressure in order to check the theoretical prediction and thus confirm the ability of the model of Section 3 to predict spectra of SO_2 under varying atmospheric conditions. The temperature dependence of the absorption coefficient per unit pressure (in a closed-off cell where the number of molecules remains constant) is shown in Fig. 5-2 for three lines in the 1117-cm^{-1} region, for a temperature range from 23 to 200°C. According to theory, the temperature dependence of the absorption constant of a single line is determined by three parameters: (a) the thermal population (or Boltzmann)

function exp[−W/kT], where W is the internal energy of the lower state, k is the Boltzmann constant, and T the absolute temperature; (b) the partition function, which varies approximately as $T^{-3/2}$; (c) the linewidth, which varies as $T^{1/2}$ for pure Doppler broadening, but is more complicated in the 1-Torr region (where the data were taken) because of pressure-broadening effects. If we assume that pressure (hence, pressure broadening) increases linearly with increasing temperature, and that the Doppler- and pressure-broadened linewidth contributions add quadratically, then the solid curves of Fig. 5-2 represent the best fit to the data for the (18,6,12) ← (19,7,13) and (13,7,7) ← (14,8,6) lines when an arbitrary scale is used. In order to obtain the fit to the points denoting the (8,8,0) ← (9,9,1) transition shown by the dashed line, the scale factor for this curve had to be increased by 15 percent over that used for the other two curves.

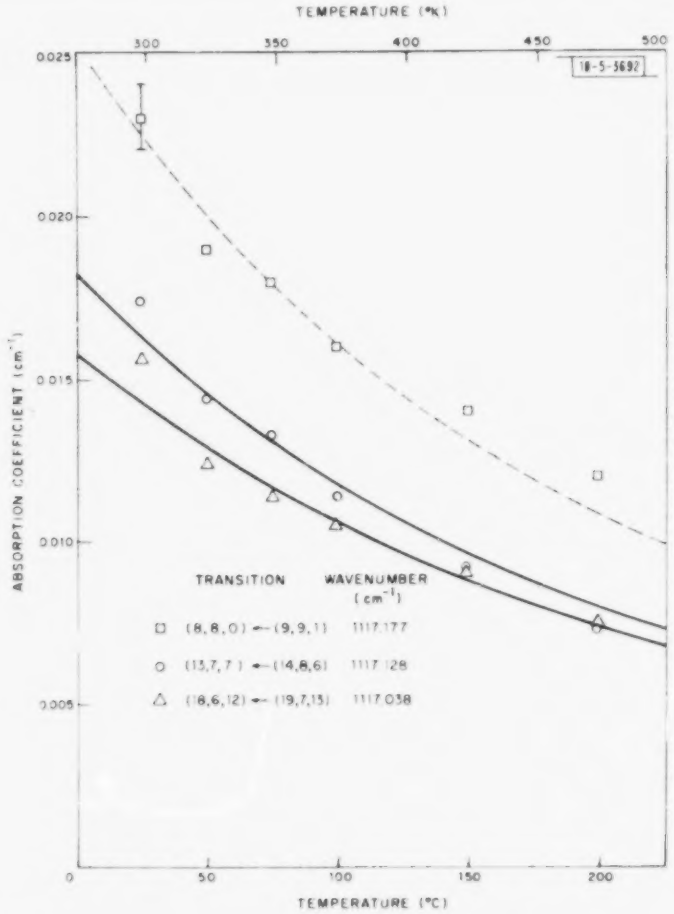

Fig. 5-2. Temperature dependence of the absorption coefficient of three SO_2 lines (identified in the legend) from 23 to 209°C. Gas pressure at room temperature was 1 Torr in each case. The solid lines represent theoretical fits to the two lower transitions; the dashed line is a theoretical fit to the third line when the vertical scale factor is increased by 15 percent (see text).

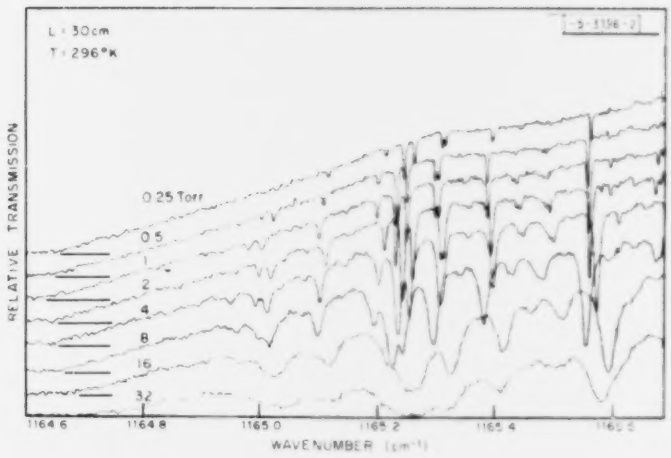

Fig. 5-3. Diode laser scans of the 1164-cm^{-1} region of SO_2 absorption for gas pressures of from 0.25 to 32 Torr. L = 30 cm, T = 296°K. (Zero-transmission lines for the different pressures were shifted vertically for clarity.)

The effect produced on spectral resolution by increasing SO_2 pressure is shown in Fig. 5-3 for pressures from 0.25 to 32 Torr. At pressures above 2 Torr, the highest resolution begins to be lost, although recognizable structure is apparent even for 16 Torr pressure. It should be noted, however, that at 16 Torr the atmospheric concentration of SO_2 would be over 20,000 ppm, which would probably not be encountered in the usual monitoring applications. The self-broadening of SO_2 lines can usually be neglected -- a conclusion also arrived at by Burch, et al.,[19] on the basis of their measurements.

Since air broadening of spectral absorption lines is usually the dominant mechanism affecting resolution and sensitivity of spectroscopic techniques, it is illustrative to consider the effect on a single absorption line of increasing air pressure to 1 atmosphere (760 Torr). An experiment was performed in which the relative concentration of NH_3 in air was maintained at 1000 ppm, and the absorption coefficient measured as a function of air pressure, as shown in Fig. 5-4. At pressures below 10 Torr, the absorption coefficient increases linearly with pressure, corresponding to the larger number of NH_3 molecules in the absorption cell in direct proportion to the number of air molecules (to maintain 1000 ppm). At air pressures above this value, the NH_3 line broadens in direct proportion to the pressure at the rate of 6.3 MHz/Torr shown in Section 3. In the pressure-broadened regime, the absorption coefficient at a frequency ν away from the line center ν_o may be approximated by the Lorentzian shape

$$\alpha(\nu, \Delta\nu, p) \simeq \frac{c_1 p_{NH_3} \Delta\nu}{4(\nu - \nu_o)^2 + (\Delta\nu)^2} \quad , \tag{5-1}$$

where c_1 is proportional to the fundamental line strength and $\Delta\nu$ is the full-width of the line at half-maximum (FWHM). In the air-broadened case, $\Delta\nu = c_2 p_{air}$ (where c_2 = 6.3 MHz/Torr), which yields, at the line center,

$$\alpha(\nu_o, \Delta\nu, p) \simeq \frac{c_1}{c_2} \frac{P_{NH_3}}{P_{air}} \quad . \tag{5-2}$$

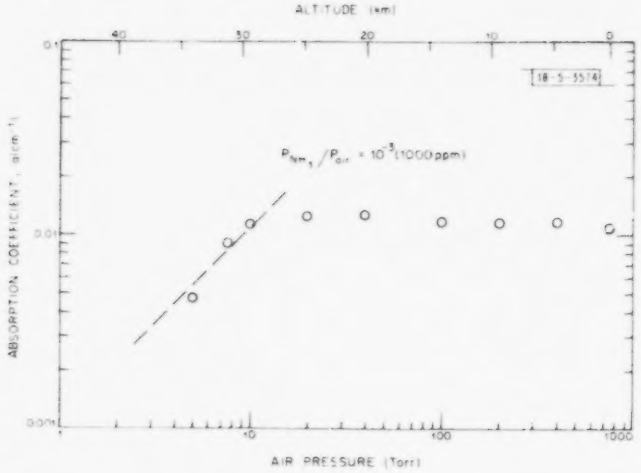

Fig. 5-4. Measured variation in the absorption coefficient of a single NH_3 line with air pressure, maintaining a fixed relative concentration of 10^{-3} (1000 ppm). Also indicated is a scale of altitude above sea level for corresponding values of air pressure.

Thus the absorption coefficient is constant for a fixed relative pollutant concentration. Also indicated in Fig. 5-4 is a scale relating the air pressure to altitude above the Earth's surface, showing the onset of full pressure-broadening effects at altitudes below 30 km.

The effect of air broadening on SO_2 lines around 1118 cm^{-1} was also studied with tunable diode laser scans. At atmospheric pressure the average absorption in this region was 30 percent for 20 Torr SO_2 (in 1 atmosphere of air) in a 30-cm-long cell. This produced a value for net line strength per unit concentration of SO_2 of 4.3×10^{-7} cm^{-1}/ppm, which is in good agreement with that value which can be derived from the grating spectrometer data.[19] In the somewhat stronger 1127-cm^{-1} region, the strength is expected to be approximately 1×10^{-6} cm^{-1}/ppm.

In an attempt to uncover any possible interferences between SO_2 absorption lines in the 1200-cm^{-1} region and those of other pollutant gases which may be usually present in the atmosphere, automobile exhaust at atmospheric pressure was introduced into the gas cell. No absorption lines were detected using a diode laser to scan the wavelength region containing several SO_2 lines, indicating that over this region the pollutant gases present in the exhaust specimen (including water vapor) do not interfere with the SO_2 determination.

5.3 Long-Path Transmission Experiment

In order to evaluate qualitatively the characteristics of diode laser transmission over relatively long atmospheric paths, collimated radiation from the laser was directed outside the laboratory to the rooftop of another building 38 meters away. A mirror on the other building re-directed the beam toward the source, where 3.8-cm-diameter collecting optics focused the radiation onto a Ge:Cu detector. Over 50 percent of the emitted laser radiation was collected after traversing the 76-meter two-way path through the atmosphere. (The experiment was preliminary, and no attempt was made to achieve ultimate optimization or to scan through regions of SO_2 absorption.) It was clear, however, that the stability of the return signal indicated negligible atmospheric scattering, with a signal-to-noise ratio of over 50:1 for the relatively low 20 μW of laser power. As has been pointed out by Kildal and Byer,[20] high-power lasers are not necessary for sensitive, long-path monitoring of the atmosphere by "resonance absorption."

ACKNOWLEDGMENTS

During the performance of the tasks described in this report, assistance was received from many individuals not directly supported by the program or involved in its implementation. Their unselfish generosity of time, knowledge, and even personal commitment helped immeasurably in meeting the program objectives.

In the semiconductor diode laser development, the contributions of A. R. Calawa are of particular importance in that he supplied the devices used during this period. Most of the crystal-growing techniques have been developed and are still being advanced by T. C. Harman.

Initial encouragement for the application of tunable diode lasers to gaseous pollutant detection came from P. L. Kelley, who has continued to give valuable advice on all aspects of the program. Helpful comments and critical appraisals were also provided by J. O. Dimmock, I. Melngailis, R. H. Rediker, and R. H. Kingston (RHK first proposed remote heterodyne detection). General encouragement and advice were also received from many other members of the Lincoln Laboratory staff.

Appreciation is expressed to S. A. Clough of the Air Force Cambridge Research Laboratories for providing theoretical band structure information on SO_2 and collaborating in the interpretation of the measured ultra-high-resolution data. D. I. Underwood of Lincoln Laboratory has performed further computer analysis of Clough's theoretical data.

For supplying recent unpublished data of the positions and strengths of NH_3 lines used for calibrating the SO_2 laser-produced spectra, we are deeply indebted to John Curtis, Peter Yin, and K. Narahari Rao of Ohio State University

REFERENCES

1. Detection of Air Pollutants with Tunable Diode Lasers, E. D. Hinkley and P. L. Kelley, Science 171, 635 (1971).

2. The Use of Lasers in Pollution Monitoring, I. Melngailis, IEEE Transactions on Geoscience Electronics (to be published).

3. Infrared Spectroscopy and Infrared Lasers in Air Pollution Research and Monitoring, P. L. Hanst, Applied Spectroscopy 24, 161 (1970).

4. Infrared Spectroscopy of CO Using a Tunable PbSSe Diode Laser, K. W. Nill, F. A. Blum, A. R. Calawa, and T. C. Harman, Appl. Phys. Lett. 19, 79 (1971).

5. Observation of Lambda Doubling and Zeeman Splitting in the Fundamental Infrared Absorption Band of Nitric Oxide, K. W. Nill, F. A. Blum, A. R. Calawa, and T. C. Harman (submitted for publication).

6. Crystal Growth, Annealing, and Diffusion of Lead-Tin Chalcogenides, A. R. Calawa, T. C. Harman, M. Finn, and P. Youtz, Trans. Met. Soc. Amer. Inst. Mining Eng. 242, 374 (1968).

7. Catalog of Infrared Spectra for Qualitative Analysis of Gases, R. H. Pierson, A. N. Fletcher, and E. St. Clair Gantz, Anal. Chem. 28, 1218 (1956).

8. I. Melngailis and T. C. Harman (private communication); see also Ref. 2.

9. The Infrared Spectrum and Molecular Constants of Sulfur Dioxide, R. D. Shelton, A. H. Nielsen, and W. H. Fletcher, J. Chem. Phys. 21, 2178 (1953).

10. Direct Observation of the Lorentzian Line Shape as Limited by Quantum Phase Noise in a Laser above Threshold, E. D. Hinkley and Charles Freed, Phys. Rev. Lett. 23, 277 (1969).

11. Vibration-Rotation Structure in Absorption Bands for the Calibration of Spectrometers from 2 to 16 Microns, E. K. Plyler, A. Danti, L. R. Blaine, and E. D. Tidwell, NBS Monograph 16, 21 June 1960. The Low-Frequency Vibration Rotation Bands of the Ammonia Molecule, J. S. Garing, H. H. Nielsen, and K. N. Rao, J. Molec. Spectros. 3, 496 (1959). Joan Curtis, Peter Yin, and K. N. Rao (private communication).

12. S. A. Clough (private communication).

13. Microwave Spectrum and Rotational Constants for the Ground State of D_2O, W. S. Benedict, S. A. Clough, L. Frenkel, and T. E. Sullivan, J. Chem. Phys. 53, 2565 (1970).

14. G. Steenbeckeliers, Ann. Soc. Sci., Bruxelles 82, 331 (1968).

15. Ozone Absorption in the 9.0 Micron Region, AFCRL Report 65-862, Physical Sciences Research Paper No. 170 (1965), S. A. Clough and F. X. Kneizys, Coriolis Interaction in the ν_1 and ν_3 Fundamentals of Ozone, S. A. Clough and F. X. Kneizys, J. Chem. Phys. 44, 1855 (1966).

16. Use of CO and CO_2 Lasers to Detect Pollutants in the Atmosphere, R. T. Menzies, Appl. Optics 10, 1532 (1971).

17. Low-Level Coherent and Incoherent Detection in the Infrared, R. J. Keyes and T. M. Quist, Chapter 8 of "Semiconductors and Semimetals," edited by R. K. Willardson and A. C. Beer (Academic Press, New York, 1970).

18. J. U. White, J. Opt. Soc. Amer. 32, 285 (1942).

19. Absorption and Emmision by SO_2 between 1050 and 1400 cm^{-1} (9.5-7.1 μm), D. E. Burch, J. D. Pembrook, and David A. Gryvnak, Final Technical Report to the Environmental Protection Agency under Contract No. 68-02-0013, July 1971.

20. Comparison of Laser Methods for the Remote Detection of Atmospheric Pollutants, H. Kildal and R. L. Byer, Proc. IEEE 59, 1644 (1971).

APPENDIX A
TUNABLE LASER SPECTRA OF THE ν_1 BAND OF SULFUR DIOXIDE

Shown here are some of the actual diode laser scans of portions of the ν_1 absorption band of SO_2 at room temperature. The NH_3 lines used for wavelength calibration are also shown, and are tabulated in Appendix C. The SO_2 scans were usually taken at three different pressures: 0.1, 1, and 10 Torr. In most instances the 1-Torr curves were used to determine the fundamental line intensities. These are tabulated in Appendix B.

Experimentally, emission from the tunable diode laser was collimated by a BaF_2 lens 3.8 cm in diameter and having a 10.6-cm focal length. The collimated radiation passed through a 30-cm-long stainless steel or pyrex cell with BaF_2 windows, thence to another lens for focusing onto the entrance slit of a grating spectrometer. The spectrometer served a twofold purpose: (1) to provide approximate wavelength information, and (2) to limit, even with wide slit positions, the passband of the optical radiation from the laser so that power in any other modes would not be detected. The detector was liquid-helium-cooled Ge:Cu. The SO_2 was of 99.98 percent purity, obtained from the Matheson Company, Inc. of East Rutherford, New Jersey. Evacuation of gas cells, detector Dewars, and laser Dewars was achieved with a turbomolecular pump. Gas pressure was measured with a capacitance manometer.

Figure A-1 shows diode laser scans for SO_2 in the region from 1114.5 to 1115.2 cm^{-1} and can be used to illustrate the procedure that was followed. The top curve corresponds to the evacuated-cell case (p = 0), and the relatively noisy horizontal line slightly above the abscissa shows the detector noise even when the laser beam is blocked, and serves as the reference for zero transmission. The bell-shaped profile of the p = 0 curve is caused mainly by the change in laser power as the diode is tuned across this mode – it is not usually caused by the spectrometer slit function, except over very wide tuning ranges. It may be noted that there appears to be a "ripple" on even the p = 0 curve; this is produced by a Fabry-Perot effect between some reflecting (or partially reflecting) surfaces illuminated by the laser beam. Although attempts are usually made to reduce these oscillations, they can be used to check linearity of tuning since they are periodic in wavelength. After the p = 0 curve has been taken, 0.1 Torr of SO_2 is placed in the cell and a second curve produced. Sequentially, the 1-Torr and 10-Torr curves for SO_2 are recorded, followed by the NH_3 calibration trace.

Laser spectroscopy permits the fundamental absorption profile of a spectral line to be observed, and its basic strength determined in accordance with the Beer-Lambert equation,

$$\alpha'_p = -\frac{1}{pL}\ln(I/I_o) \quad . \tag{A-1}$$

Here, I/I_o is the fractional transmission at the line center, p the gas pressure, L the cell length, and α'_p the absorption coefficient per unit pressure (one measure of line "intensity").

Because of a relatively high rate of self-broadening (40 MHz/Torr for FWHM) coupled with a relatively narrow Doppler width as a result of a large molecular weight, pressure broadening of SO_2 spectral lines is noticeable even at pressures as low as 1 Torr. The Doppler width can be calculated from the equation

$$\Delta\nu_D = \frac{215}{\lambda}\sqrt{T/MW} \quad , \tag{A-2}$$

where, if T is in °K, the molecular weight in grams, and λ in μm, the Doppler width is in units of MHz. For SO_2 at room temperature, the Doppler width (FWHM) is 53 MHz at 8.7 μm. At a

self-broadening rate of 40 MHz/Torr, noticeable increases in the linewidths will occur for SO_2 pressure above about 0.15 Torr, becoming approximately 66 MHz at 1 Torr, or 1.24 times larger than the Doppler width. Since the absorption constant (per unit pressure) of Eq. (A-1) varies inversely with linewidth, values arrived at on the basis of measurements made at 1-Torr pressure must be increased by 1.24 in order to give data corresponding to the Doppler limit. This adjustment was made in reducing the data from Figs. A-1 through A-20 to the form shown in Appendix B.

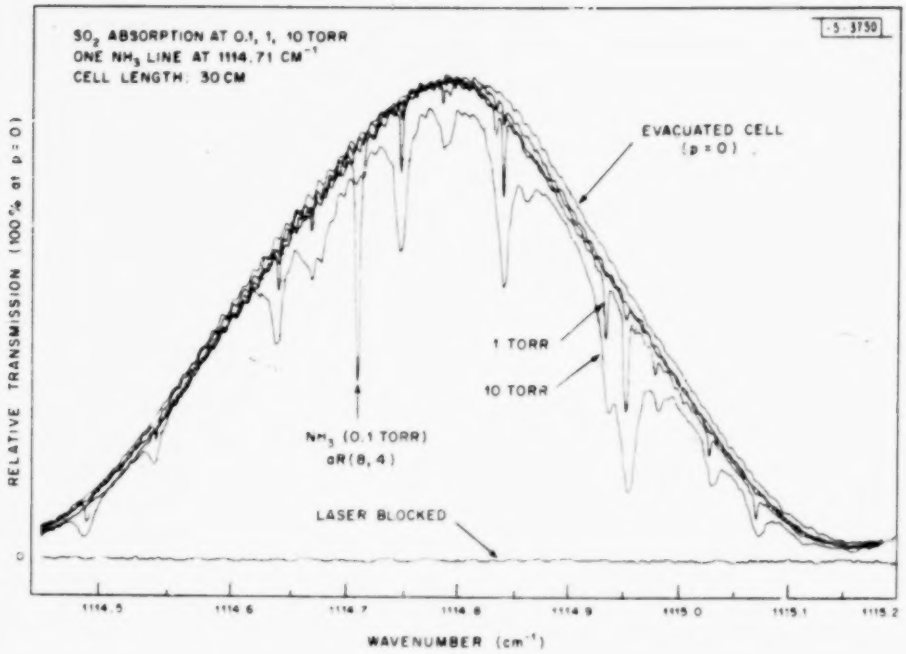
SO_2 ABSORPTION AT 0.1, 1, 10 TORR
ONE NH_3 LINE AT 1114.71 CM^{-1}
CELL LENGTH: 30 CM
5-3750
EVACUATED CELL
(p = 0)
1 TORR
10 TORR
NH_3 (0.1 TORR)
aR(8,4)
LASER BLOCKED
RELATIVE TRANSMISSION (100% at p = 0)
0
1114.5
1114.6
1114.7
1114.8
1114.9
1115.0
1115.1
1115.2
WAVENUMBER (cm^{-1})

Fig. A-1.

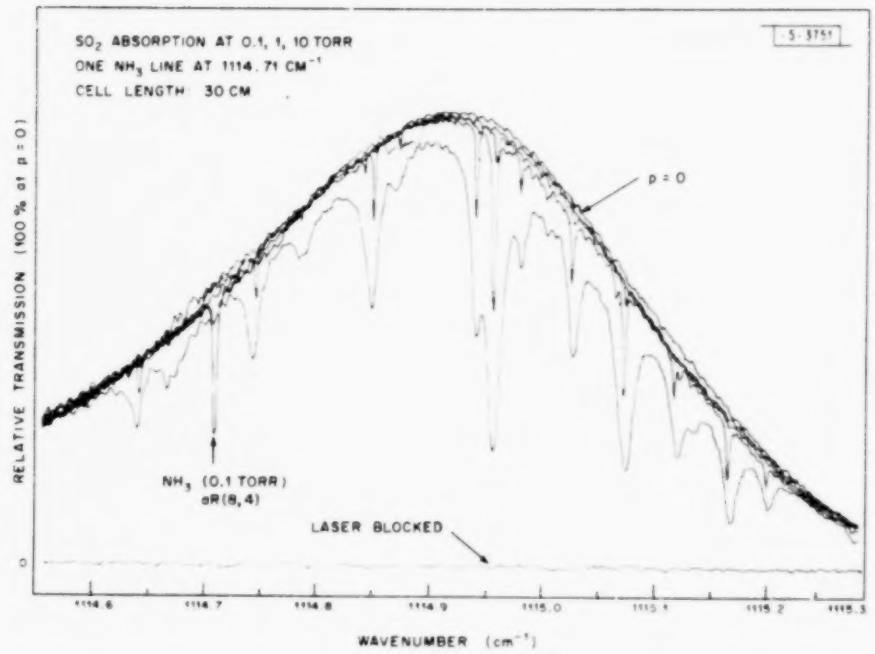
SO_2 ABSORPTION AT 0.1, 1, 10 TORR
ONE NH_3 LINE AT 1114.71 CM^{-1}
CELL LENGTH: 30 CM
5-3751
p = 0
NH_3 (0.1 TORR)
aR(8,4)
LASER BLOCKED
RELATIVE TRANSMISSION (100% at p = 0)
0
1114.6
1114.7
1114.8
1114.9
1115.0
1115.1
1115.2
1115.3
WAVENUMBER (cm^{-1})

Fig. A-2.

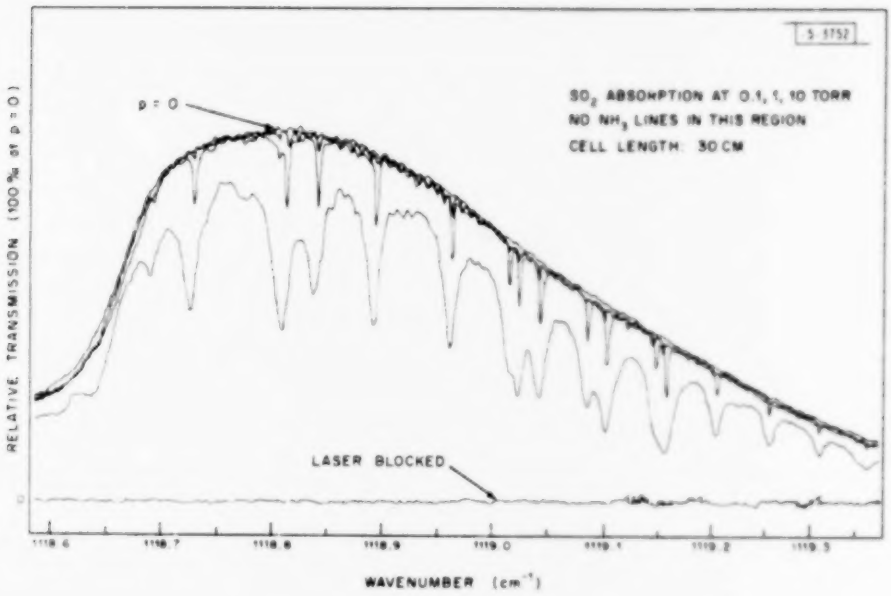
S 5752
SO_2 ABSORPTION AT 0.1, 1, 10 TORR
NO NH_3 LINES IN THIS REGION
CELL LENGTH 30 CM
p = 0
LASER BLOCKED
RELATIVE TRANSMISSION (100% at p = 0)
WAVENUMBER (cm^{-1})

Fig. A-3.

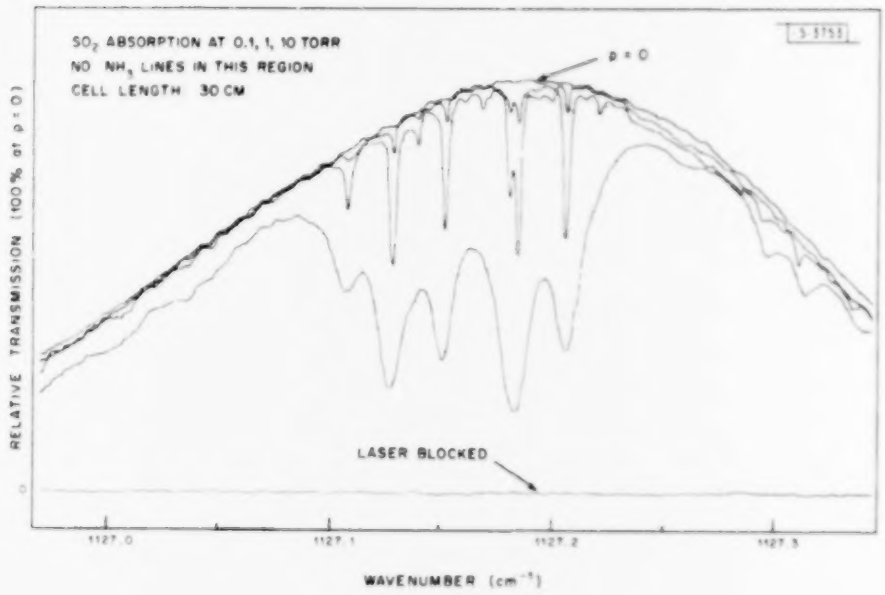
S 5753
SO_2 ABSORPTION AT 0.1, 1, 10 TORR
NO NH_3 LINES IN THIS REGION
CELL LENGTH 30 CM
p = 0
LASER BLOCKED
RELATIVE TRANSMISSION (100% at p = 0)
WAVENUMBER (cm^{-1})

Fig. A-4.

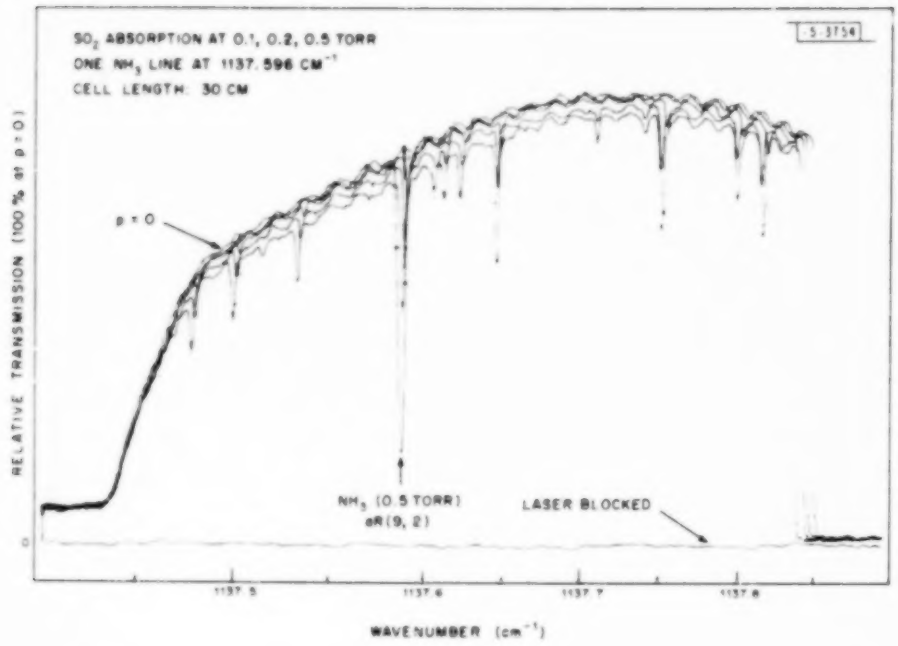
SO_2 ABSORPTION AT 0.1, 0.2, 0.5 TORR
ONE NH_3 LINE AT 1137.596 CM^{-1}
CELL LENGTH: 30 CM
5-3754
p = 0
NH_3 (0.5 TORR)
aR(9, 2)
LASER BLOCKED
RELATIVE TRANSMISSION (100% at p = 0)
0
1137.5
1137.6
1137.7
1137.8
WAVENUMBER (cm^{-1})

Fig. A-5.

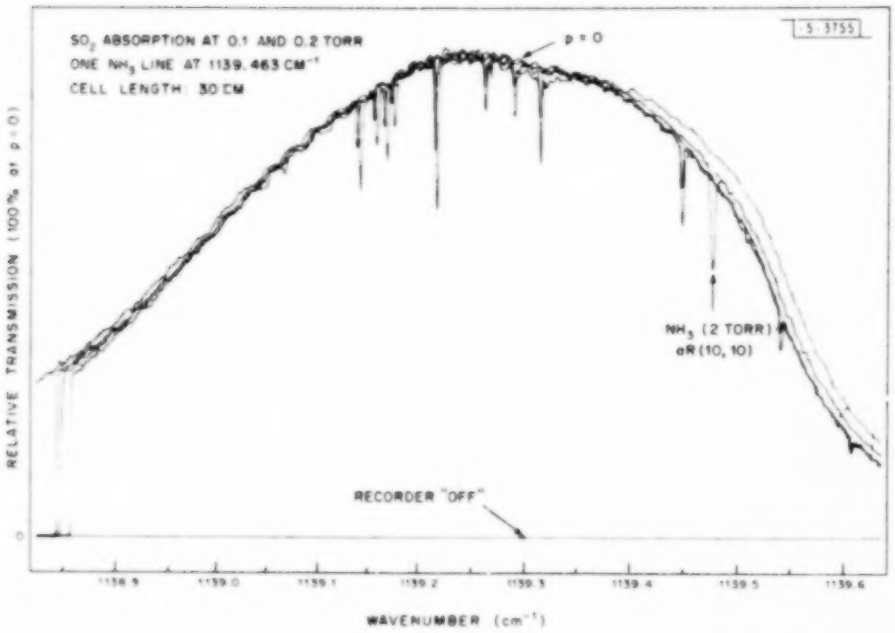
SO_2 ABSORPTION AT 0.1 AND 0.2 TORR
ONE NH_3 LINE AT 1139.463 CM^{-1}
CELL LENGTH: 30 CM
5-3755
p = 0
NH_3 (2 TORR)
aR(10, 10)
RECORDER "OFF"
RELATIVE TRANSMISSION (100% at p = 0)
0
1138.9
1139.0
1139.1
1139.2
1139.3
1139.4
1139.5
1139.6
WAVENUMBER (cm^{-1})

Fig. A-6.

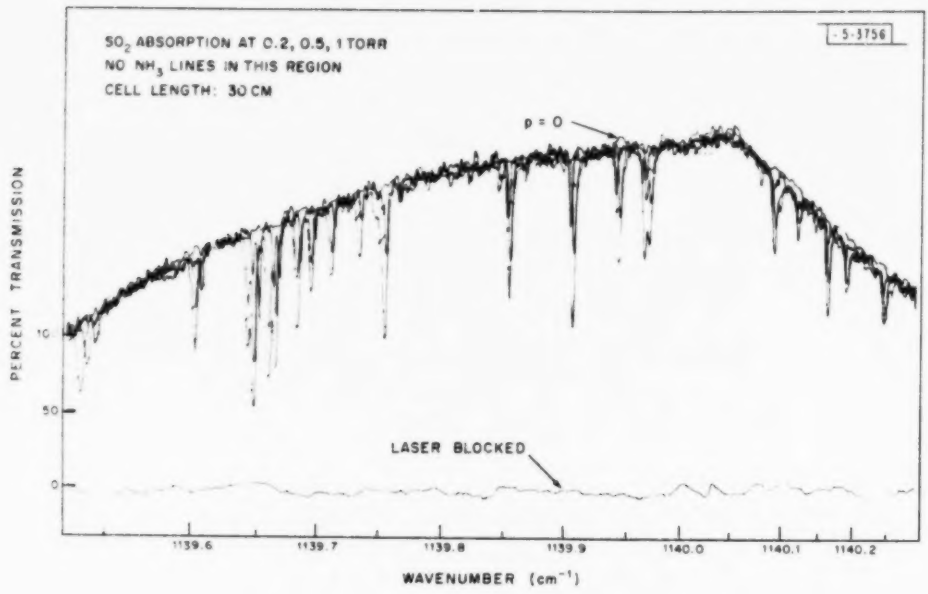
SO_2 ABSORPTION AT 0.2, 0.5, 1 TORR
NO NH_3 LINES IN THIS REGION
CELL LENGTH: 30 CM
I-5-3756
p = 0
LASER BLOCKED
PERCENT TRANSMISSION
100
50
0
1139.6
1139.7
1139.8
1139.9
1140.0
1140.1
1140.2
WAVENUMBER (cm^{-1})

Fig. A-7.

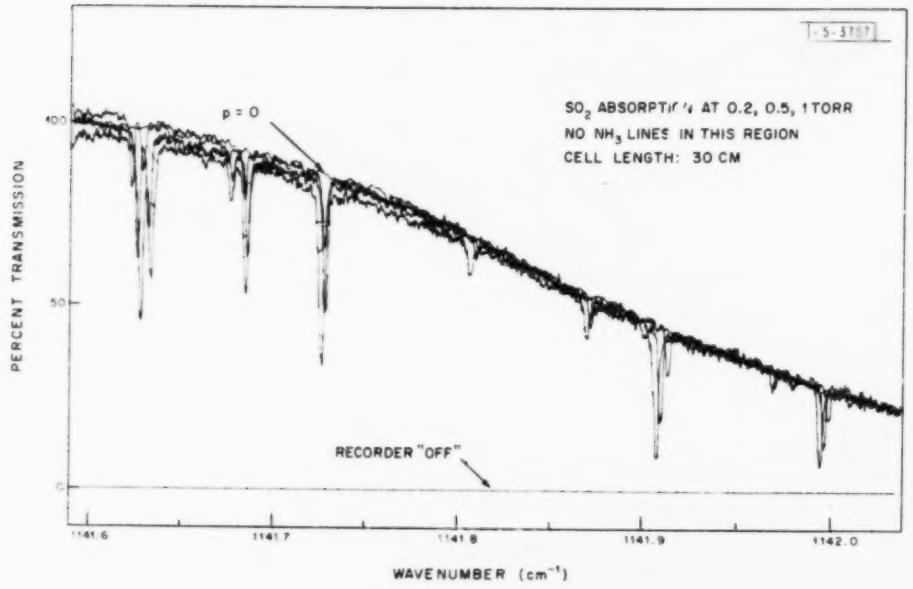
I-5-3787
p = 0
SO_2 ABSORPTION AT 0.2, 0.5, 1 TORR
NO NH_3 LINES IN THIS REGION
CELL LENGTH: 30 CM
RECORDER "OFF"
PERCENT TRANSMISSION
100
50
0
1141.6
1141.7
1141.8
1141.9
1142.0
WAVENUMBER (cm^{-1})

Fig. A-8.

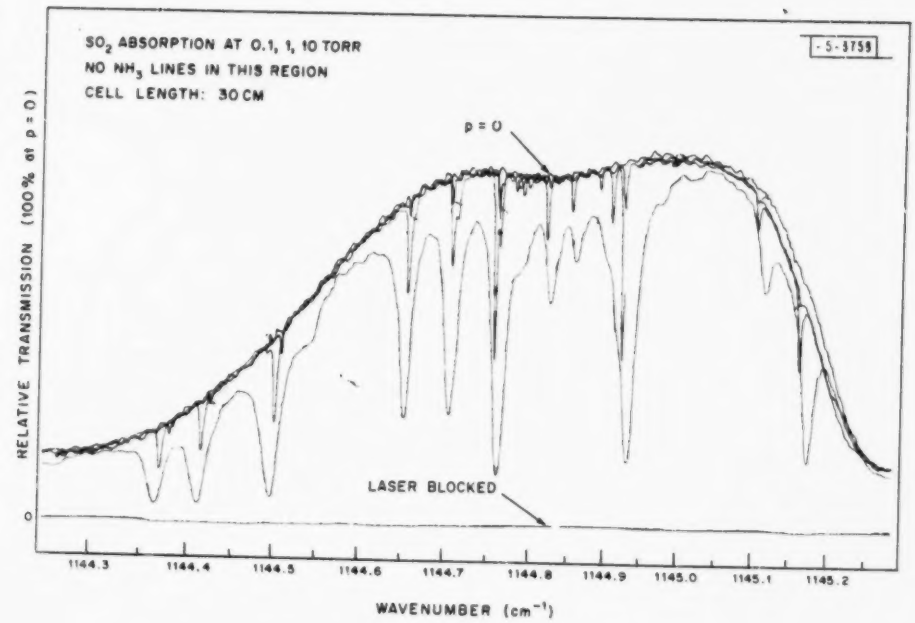

Fig. A-9.

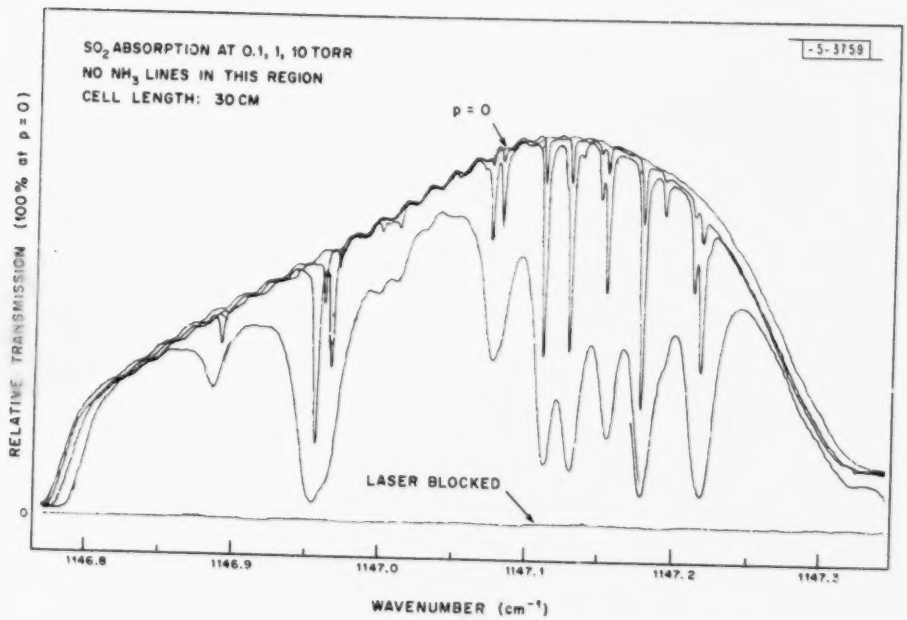

Fig. A-10.

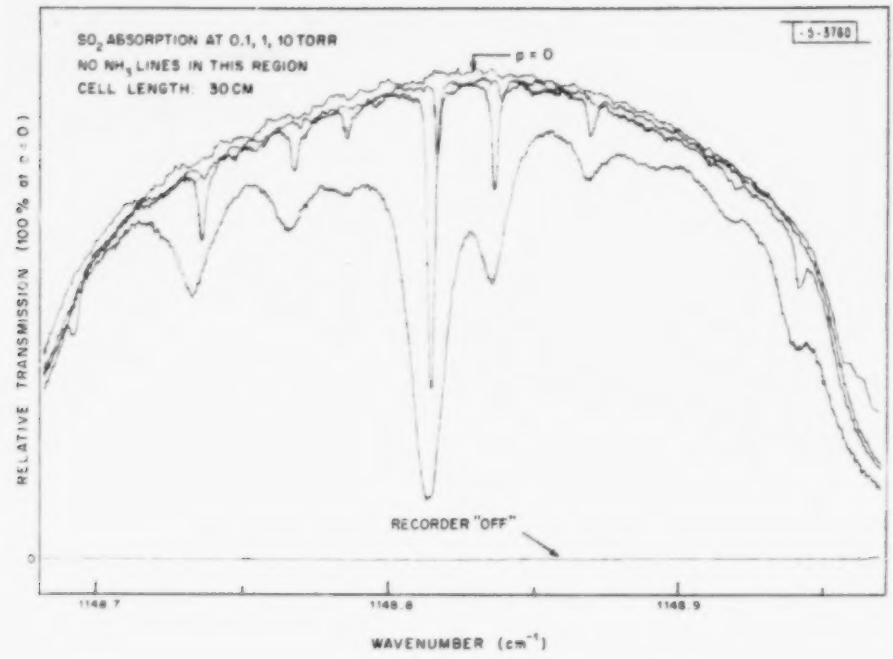

Fig. A-11.

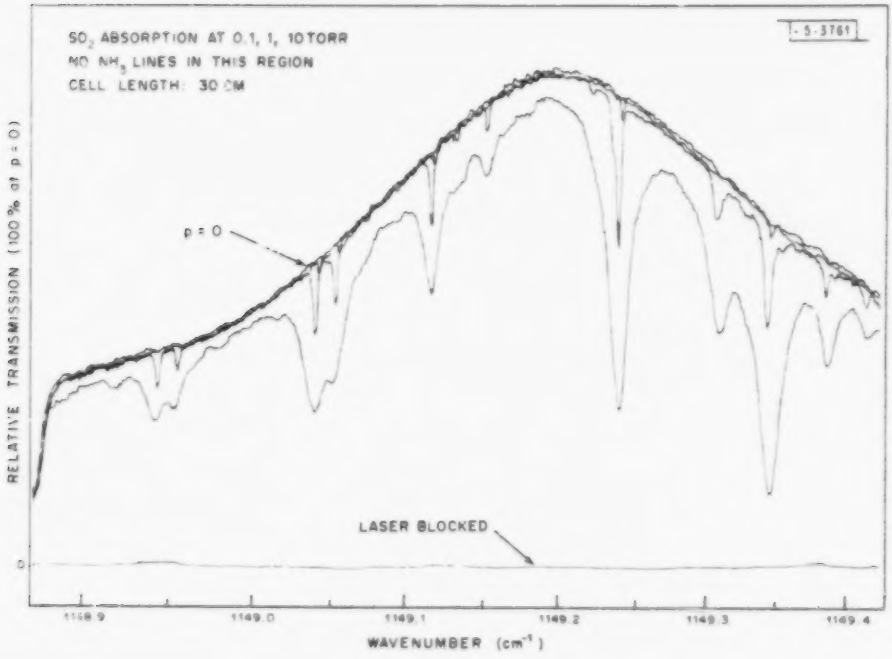

Fig. A-12.

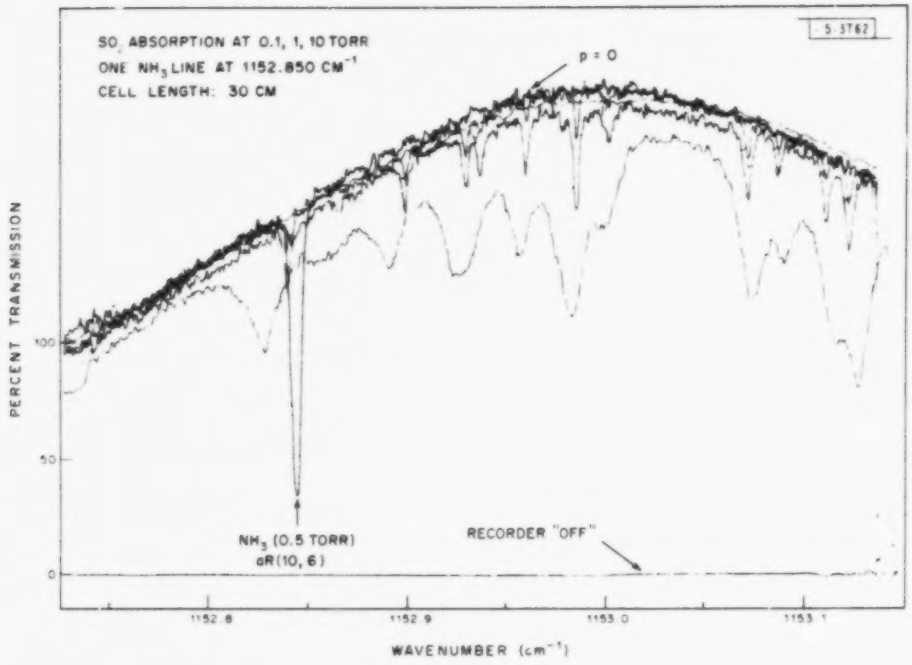

Fig. A-13.

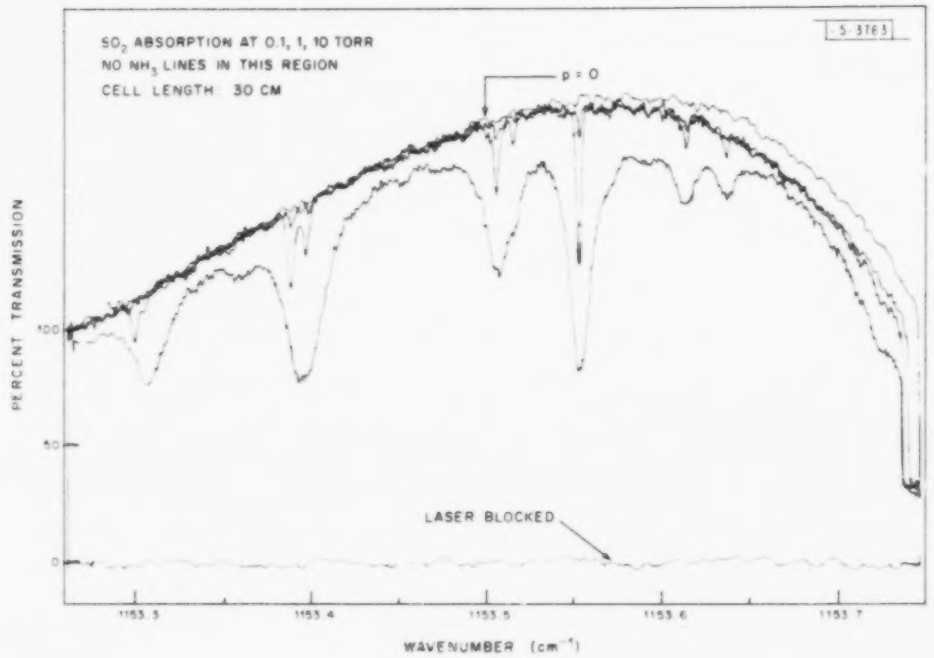

Fig. A-14.

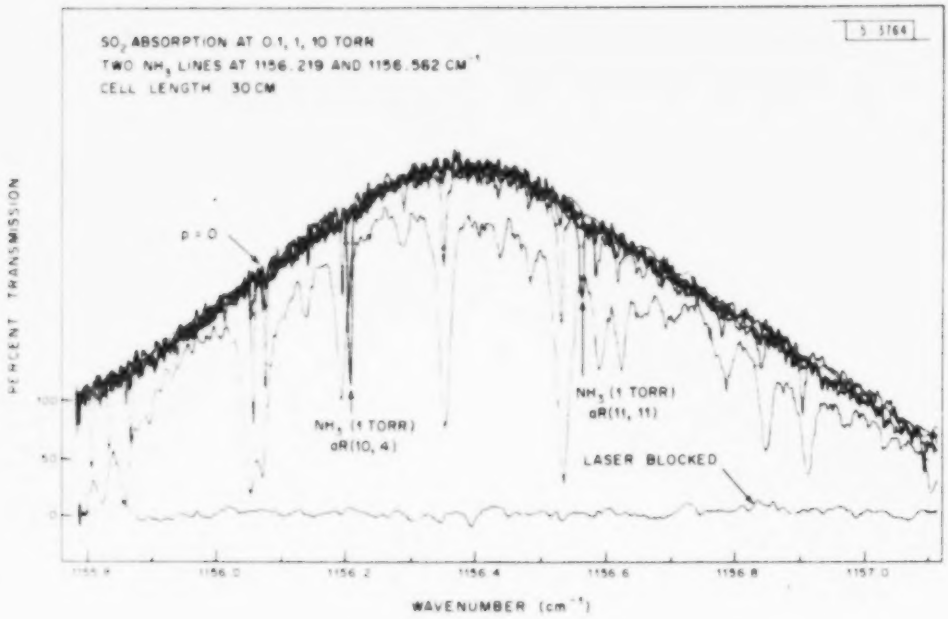

Fig. A-15.

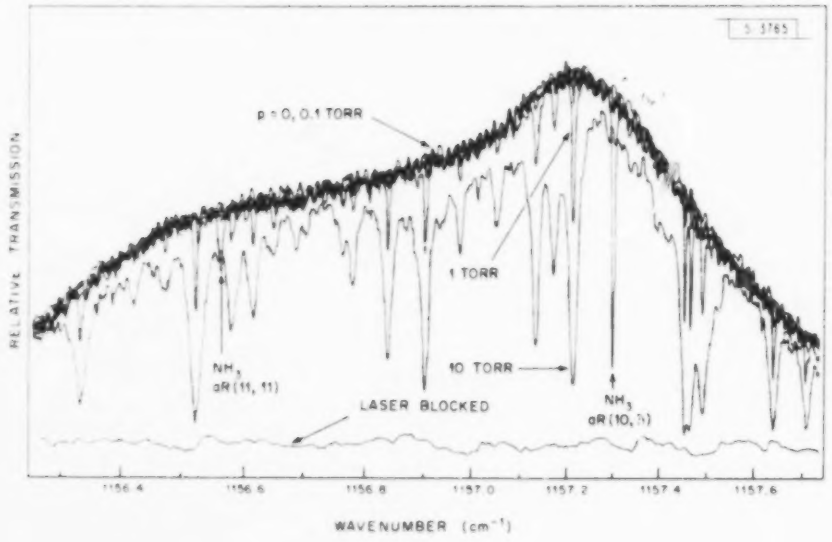

Fig. A-16.

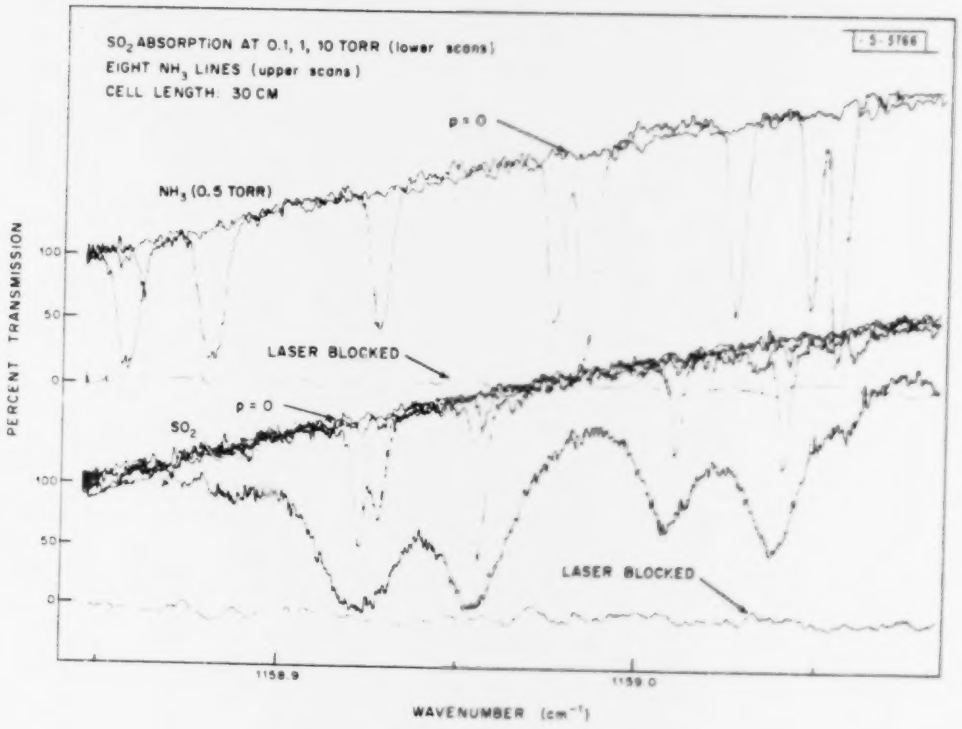

Fig. A-17.

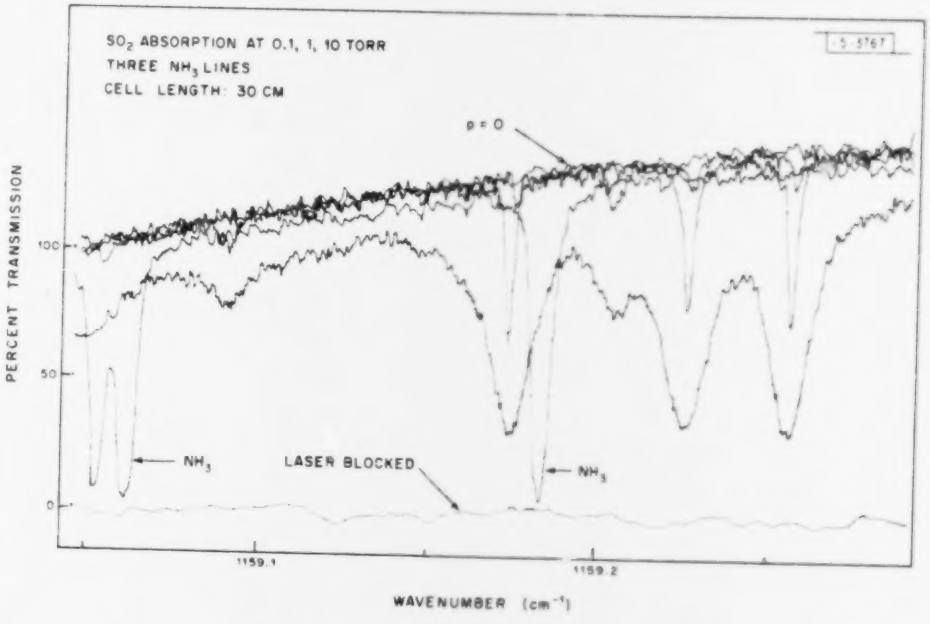

Fig. A-18.

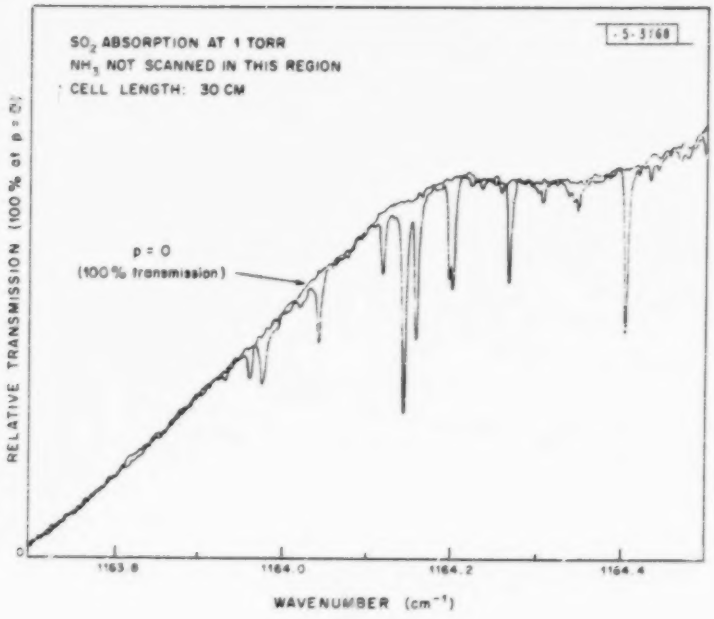

Fig. A-19.

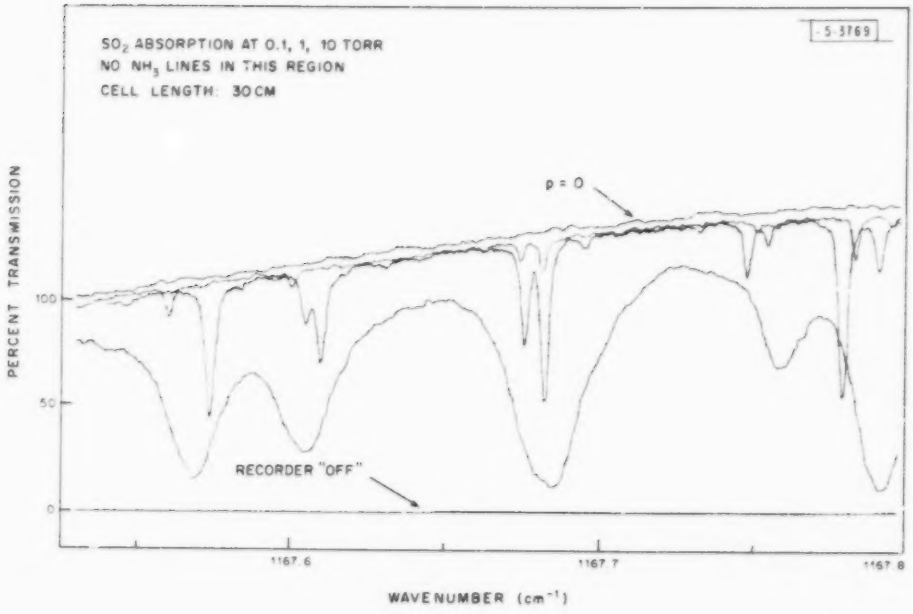

Fig. A-20.

APPENDIX B
TABULATION OF SULFUR DIOXIDE SPECTRAL DATA

On the following pages are shown the positions, intensities, and identifications of the SO_2 lines displayed in the tunable diode laser scans of Appendix A.

The wavenumber assigned to each line corresponds to its theoretical value based on a band center of 1151.71 cm^{-1}. The position of the band center was deduced from diode laser scans of regions containing both SO_2 and NH_3 absorption lines and should be accurate to ± 0.01 cm^{-1}.

The intensity of each line is listed in units of cm^{-1}/Torr and represents the fundamental value in the Doppler-broadened regime.

Identification of each line is provided by the upper and lower energy level quantum numbers (J', K'_A, K'_C) and (J'' K''_A, K''_C), respectively.

Transition* (J', K'_A, K'_C)←→(J'' K''_A, K''_C)	Wavenumber	Intensity
(12,08,04)←→(13,09,05)	1114.489 cm^{-1}	0.024 cm^{-1}/Torr
(35,10,26)←→(35,11,25)	.550	0.008
(34,10,24)←→(34,11,23)	.650	0.007
unknown	.670	0.003
(33,10,24)←→(33,11,23)	.749	0.007
unknown	.787	0.002
unknown	.793	0.001
unknown	.836	0.003
(32,10,22)←→(32,11,21)	.845	0.008
(24,15,09)←→(23,16,08)	.864	0.001
(31,10,22)←→(31,11,21)	.939	0.011
(26,05,21)←→(27,06,22) | (21,06,16)←→(22,07,15)	.954	0.022
unknown	.982	0.004
(30,10,20)←→(30,11,19)	1115.031	0.010
(16,07,09)←→(17,08,10)	.073	0.022
(29,10,20)←→(29,11,19)	.120	0.009
(11,08,04)←→(12,09,03)	.166	0.021
(28,10,18)←→(28,11,17)	.207	0.014
(27,10,18)←→(27,11,17)	.291	0.021
(25,09,17)←→(25,10,16)	1118.741	0.007
(24,09,15)←→(24,10,14)	.815	0.010
(25,04,22)←→(26,05,21)	.838	0.009
(23,09,15)←→(23,10,14)	.887	0.009
(22,09,13)←→(22,10,12)	.956	0.010
(26,04,22)←→(27,05,23)	1119.013	0.008
(21,09,13)←→(21,10,12)	.022	0.010
(20,05,15)←→(21,06,16)	.042	0.012
(20,09,11)←→(20,10,10)	.086	0.010
(15,06,10)←→(16,07,09)	.102	0.014
(19,09,11)←→(19,10,10)	.148	0.009
(10,07,03)←→(11,08,04)	.156	0.017
(18,09,09)←→(18,10,08)	.206	0.009
(17,09,09)←→(17,10,08)	.262	0.008
(16,09,07)←→(16,10,06)	.315	0.007

* Following conventional spectroscopic notation where the upper state is listed first, (→) represents the direction for emission, and (←) represents absorption.

Transition* $(J', K'_A, K'_C) \leftarrow\rightarrow (J'', K''_A, K''_C)$	Wavenumber	Intensity
(19,02,18)←→(20,03,17)	1127.108 cm^{-1}	0.008 cm^{-1}/Torr
(37,01,37)←→(38,00,38)	.129	0.020
(29,12,18)←→(28,13,15)	.151	0.017
(36,01,35)←→(37,02,36)	.152	
(17,01,17)←→(18,02,16)	.166	0.002
(34,02,32)←→(35,03,33)	.182	0.014
(08,05,03)←→(09,06,04)	.183	0.023
(13,04,10)←→(14,05,09)	.205	0.020
unknown	.293	0.003
unknown	.310	0.004
(08,02,06)←→(09,03,07)	1137.481	0.029
(30,01,29)←→(30,02,28)	.505	0.026
(25,01,25)←→(25,02,24)	.537	0.021
(18,01,17)←→(19,02,18)	.591	0.040
(29,04,26)←→(30,03,27)	.628	0.015
(27,03,25)←→(27,04,24)	.651	0.034
(13,06,08)←→(12,07,05)	.715	0.005
(27,02,26)←→(27,03,25)	.757	0.029
(40,03,37)←→(40,04,36)	.810	0.018
(34,04,30)←→(34,05,29)	.828	0.023
(19,03,17)←→(19,04,16)	1139.147	0.041
(28,01,27)←→(28,02,26)	.162	0.024
(14,01,13)←→(15,02,14)	.169	0.031
(38,03,35)←→(38,04,34)	.179	0.018
(19,01,19)←→(20,00,20)	.215	0.065
(23,03,21)←→(24,02,22)	.265	0.021
(05,02,04)←→(06,03,03)	.293	0.021
(17,03,15)←→(17,04,14)	.321	0.039
(15,03,13)←→(15,04,12)	.447	0.039
(13,03,11)←→(13,04,10)	.539	0.027
(11,03,09)←→(11,04,08)	.609	0.022
(12,03,09)←→(12,04,08)	.648	0.028
(18,00,18)←→(19,01,19)	.653	0.060
(10,03,07)←→(10,04,06)	.663	0.040
(09,03,07)←→(09,04,06)	.664	
(14,03,11)←→(14,04,10)	.669	0.033
(23,02,22)←→(23,03,21)	.685	0.022
(08,03,05)←→(08,04,04)	.695	0.017
(07,03,05)←→(07,04,04)	.709	0.014
(06,03,03)←→(06,04,02)	.730	0.016
(28,08,20)←→(27,09,19)	.744	0.016
(05,03,03)←→(05,04,02)	.745	
(16,03,13)←→(16,04,12)	.748	0.045
(04,03,01)←→(04,04,00)	.760	0.010
(19,02,18)←→(20,01,19)	.853	0.029
(18,03,15)←→(18,04,14)	.910	0.029
(12,01,11)←→(13,02,12)	.948	0.020
(21,01,21)←→(21,02,20)	.970	0.013
(04,02,02)←→(05,03,03)	.973	0.015
(32,02,30)←→(32,03,29)	1140.095	0.018
(27,04,24)←→(28,03,25)	.125	0.009
(20,03,17)←→(20,04,16)	.164	0.034
(22,00,22)←→(22,01,21)	.192	0.018
(36,03,33)←→(36,04,32)	.248	0.020

* Following conventional spectroscopic notation where the upper state is listed first, (→) represents the direction for emission, and (←) represents absorption.

Transition* $(J'K'_A, K'_C) \leftarrow\!\rightarrow (J''K''_A, K''_C)$	Wavenumber	Intensity
(17,02,16)←→(18,01,17)	1141.634 cm^{-1}	0.032 cm^{-1}/Torr
(08,01,07)←→(09,02,08)	.639	0.022
(14,05,09)←→(13,06,08)	.681	0.006
(20,00,20)←→(20,01,19)	.689	0.024
(17,02,16)←→(17,03,15)	.727	0.040
(31,05,27)←→(32,04,28)	.807	0.008
(20,06,14)←→(19,07,13)	.872	0.009
(15,01,15)←→(16,00,16)	.909	0.067
(14,00,14)←→(15,01,15)	1142.005	0.062
(18,02,16)←→(18,03,15)	1144.362	0.025
(22,02,20)←→(22,03,19)	.403	0.022
(20,02,18)←→(20,03,17)	.477	0.025
(16,00,16)←→(16,01,15)	.617	0.014
(11,01,11)←→(11,02,10)	.672	0.012
(11,01,11)←→(12,00,12)	.735	0.030
(02,01,01)←→(03,02,02)	.742	0.010
(08,03,05)←→(07,04,04)	.805	0.008
(25,06,20)←→(24,07,17)	.806	
(31,07,25)←→(30,08,22)	.841	0.004
(23,04,20)←→(24,03,21)	.890	0.006
(20,01,19)←→(20,02,18)	.904	0.031
(14,04,10)←→(13,05,09)	1145.084	0.005
(08,00,08)←→(09,01,09)	.144	0.020
(17,04,14)←→(16,05,11)	1146.899	0.008
(14,01,13)←→(14,02,12)	.956	0.051
(41,08,34)←→(42,07,35)	.964	0.024
(06,01,05)←→(06,02,04)	.965	
(23,05,19)←→(22,06,16)	1147.073	0.011
(26,04,22)←→(27,03,25)	.074	
(21,04,18)←→(22,03,19)	.080	0.010
(12,00,12)←→(12,01,11)	.110	0.038
(08,01,07)←→(08,02,06)	.128	0.034
(35,07,29)←→(34,08,26)	.129	
(29,06,24)←→(28,07,21)	.151	0.005
(04,00,04)←→(05,01,05)	.153	0.020
(12,01,11)←→(12,02,10)	.177	0.047
(28,05,23)←→(29,04,26)	.194	0.006
(11,02,10)←→(12,01,11)	.212	0.015
(10,01,09)←→(10,02,08)	.218	0.030
(22,04,18)←→(23,03,21)	1148.736	0.009
(30,06,24)←→(31,05,27)	.768	0.005
(08,00,08)←→(08,01,07)	.810	0.044
(20,04,16)←→(19,05,15)	.835	0.011
(38,07,31)←→(37,08,30)	.873	0.004
(26,05,21)←→(25,06,20)	.942	0.008
(32,06,26)←→(31,07,25)	.957	0.005
(09,02,08)←→(10,01,09)	1149.034	0.011
(15,03,13)←→(14,04,10)	.046	0.009
(19,04,16)←→(20,03,17)	.107	0.008
(34,07,27)←→(35,06,30)	.151	0.002
(29,06,24)←→(30,05,25)	.241	0.016
(05,01,05)←→(06,00,06)	.242	
(21,04,18)←→(20,05,15)	.310	0.005
(06,00,06)←→(06,01,05)	.346	0.015
(00,00,00)←→(01,01,01)	.389	0.005

* Following conventional spectroscopic notation where the upper state is listed first, (→) represents the direction for emission, and (←) represents absorption.

Transition* $(J', K'_A, K'_C) \leftrightarrow (J'', K''_A, K''_C)$	Wavenumber	Intensity
(20,05,15)←(21,04,18)	1152.850 cm^{-1}	0.009 cm^{-1}/Torr
unknown	.900	0.006
(32,05,27)←(31,06,26)	.931	0.006
unknown	.938	0.005
(33,05,29)←(32,06,26)	.962	0.005
(14,02,12)←(13,03,11)	.984	0.011
(39,06,34)←(38,07,31)	1153.004	0.003
(26,04,22)←(25,05,21)	.069	0.008
(29,07,23)←(30,06,24)	.086	0.005
(23,03,21)←(22,04,18)	.111	0.009
(20,03,17)←(19,04,16)	.123	0.010
(10,03,07)←(11,02,10)	1153.299	0.007
(09,03,07)←(10,02,08)	.363	0.010
(24,06,18)←(25,05,21)	.371	0.006
(19,05,15)←(20,04,16)	.450	0.008
(02,01,01)←(02,00,02)	.489	0.018
(33,08,26)←(34,07,27)	.557	0.005
(14,02,12)←(14,01,13)	1155.813	0.044
(12,01,11)←(12,00,12)	.837	0.029
(10,02,08)←(10,01,09)	.867	0.031
(16,02,14)←(16,01,15)	1156.058	0.042
(08,02,06)←(08,01,07)	.078	0.027
(36,05,31)←(35,06,30)	.079	
(05,01,05)←(04,00,04)	.195	0.012
(20,06,14)←(21,05,17)	.337	0.020
(30,04,26)←(29,05,25)	.521	0.023
(18,02,16)←(18,01,17)	.523	
(04,02,02)←(04,01,03)	1156.580	0.007
(18,02,16)←(17,03,15)	.616	0.008
(24,03,21)←(23,04,20)	.780	0.004
(14,01,13)←(14,00,14)	.842	0.014
(10,00,10)←(09,01,09)	.911	0.015
(07,01,07)←(06,00,06)	1157.142	0.010
(05,02,04)←(05,01,05)	.183	0.006
(20,02,18)←(20,01,19)	.222	0.022
(22,03,19)←(22,02,20)	.442	0.029
(24,03,21)←(24,02,22)	.455	0.027
(14,01,13)←(13,02,12)	.479	0.022
(07,02,06)←(07,01,07)	.481	
(20,03,17)←(20,02,18)	.643	0.030
(26,03,23)←(26,02,24)	.717	0.020
(11,01,11)←(10,00,10)	1158.924	0.046
(30,04,26)←(30,03,27)	.931	0.029
(13,02,12)←(13,01,13)	.954	0.056
(14,03,11)←(14,02,12)	.955	
(36,04,32)←(36,03,33)	1159.013	0.020
(30,03,27)←(30,02,28)	.041	0.025
(16,01,15)←(15,02,14)	1159.170	0.026
(18,01,17)←(18,00,18)	.224	0.022
(24,02,22)←(24,01,23)	.258	0.027

* Following conventional spectroscopic notation where the upper state is listed first, (→) represents the direction for emission, and (←) represents absorption.

Transition* $(J', K'_A, K'_C) \leftarrow (J'', K''_A, K''_C)$	Wavenumber	Intensity
(38,03,35)←(38,02,36)	1163.988 cm^{-1}	0.007 cm^{-1}/Torr
(25,02,24)←(25,01,25)	.996	0.011
(06,03,03)←(05,02,04)	1164.050	0.012
(26,01,25)←(26,00,26)	.118	0.008
(22,00,22)←(21,01,21)	.140	0.038
(17,02,16)←(16,01,15)	.154	0.021
(31,04,28)←(31,03,29)	.194	0.013
(29,03,27)←(29,02,28)	.198	0.014
(26,02,24)←(25,03,23)	.263	0.013
(28,05,23)←(28,04,24)	.413	0.023
(32,02,30)←(32,01,31)	.413	
(28,01,27)←(27,02,26)	1167.575	0.037
(39,06,24)←(39,05,35)	.605	0.012
(13,03,11)←(12,02,10)	.606	
unknown	.611	0.022
(30,02,28)←(29,03,27)	.674	0.021
(27,02,26)←(26,01,25)	.681	0.039
(37,03,35)←(37,02,36)	.751	0.010
(46,07,39)←(46,06,40)	.755	0.003
(29,01,29)←(28,00,28)	.786	0.041
(37,06,32)←(37,05,33)	.802	0.010

* Following conventional spectroscopic notation where the upper state is listed first, (→) represents the direction for emission, and (←) represents absorption.

APPENDIX C

NH_3 CALIBRATION LINES FOR THE 1100-1200 CM^{-1} REGION

The table below lists some of the NH_3 lines used to calibrate the wavelength scale for the tunable diode laser scans of the SO_2 absorption lines in the ν_1 band. Where possible, the actual lines have been identified and their fundamental (Doppler-limited) intensities measured.

Line*	Wavenumber (cm^{-1})	Intensity (cm^{-1}/Torr)
aR(8,4)	1114.71	0.25
--	--	--
aR(9,2)	1137.596	0.09
aR(9,1)	1138.082	
aR(10,10)	1139.463	0.005
--	--	--
aR(10,9)	1143.905	
aR(10,8)	1147.538	
aR(10,7)	1150.460	
aR(10,6)	1152.850	0.10
aR(10,5)	1154.734	
aR(10,4)	1156.219	0.03
aR(11,11)	1156.562	0.01
aR(10,3)	1157.288	0.05
aR(10,2)	1158.044	
Identification not established at this time (from laser scans)	1158.859	0.15
	.882	0.13
	.927	0.08
	.975	0.08
	1159.027	0.09
	.048	0.08
	.055	0.17

* (Line identification follows that of Ref. 11 (G, N,& R) of text.)

APPENDIX D
DETECTION OF AIR POLLUTANTS WITH TUNABLE DIODE LASERS*

E. D. Hinkley and P. L. Kelley

Sensitive, specific detection of pollutant gases can be obtained with tunable semiconductor lasers.

In this paper we describe the use of tunable $Pb_{1-x}Sn_xTe$ semiconductor diode lasers in remote or long-range sensing and point sampling of molecular pollutant gases. Remote sensing can be accomplished by measurements of the infrared absorption or emission lines characteristic of a particular pollutant at atmospheric pressure. Point sampling permits gas pressures to be reduced until the Doppler-broadened infrared absorption structure is revealed, thereby making possible very good specificity. Since one measurement technique is used for all the pollutant gases, the operational requirements are simplified. Moreover, the essentially instantaneous response is advantageous for a number of applications.

Several optical techniques for the detection of pollutant gases are currently being explored in various laboratories. They range from classical methods using selective filters, spectrographs, interferometers, and optical-correlation instruments,[1] to the use of lasers for direct absorption[2] and Raman scattering.[3] One advantage of optical sensing[4] over conventional wet chemical methods is that the measurements can be performed *in situ* by measuring emission spectra, detecting scattered laser radiation, or by transmission measurements over relatively long atmospheric paths. Infrared spectroscopy is considered an important technique since each of the major molecular pollutants contains at least one strong band in the 3-15 μm region. Dispersive infrared instruments currently used in the field usually have resolutions which are much poorer than the linewidths of typical gases at atmospheric pressure, and potentially useful information is lost. Even when high-quality spectrometers are used, the resolving power must usually be reduced in order to maintain a reasonable signal-to-noise ratio with the relatively low power per unit spectral range available from incoherent sources.

The use of gas lasers as nondispersive instruments, on the other hand, is severely restricted by the inability to "tune" these lasers appreciably from their nominal wavelengths – and the match to pollutant gas absorption lines is seldom ideal.[2]

Diode lasers of $Pb_{1-x}Sn_xTe$ can be "tailored" chemically, by adjusting the composition factor "x," to emit anywhere in the wavelength range from 6.5 to 32 μm (Ref. 5), thereby permitting an ideal match to the strong infrared absorption lines of most of the molecular pollutant gases. Tuning of individual lead-salt lasers can be achieved by application of pressure,[6] an external magnetic field,[7] or by varying the laser temperature.[8] In a simple manifestation of temperature-tuning, a laser can be tuned over a range of 40 cm^{-1} quasi-continuously (from one continuously tunable mode to another) by changing the diode current. This tuning range is sufficient to identify the spectral signature of a given pollutant even in the presence of other molecular species, and to permit a quantitative determination of its concentration. These features overcome the major limitations of conventional gas lasers in monitoring applications.

---

* Published in Science 171, 635 (1971).

Other tunable laser sources may also be useful for air pollution monitoring. These include the spin-flip Raman lasers,[9] organic dye lasers, and systems involving parametric oscillators or difference frequency generators. At the present time these devices are much more complex than the tunable semiconductor diode lasers; nevertheless, their wide tuning ranges should soon find many applications in the more conventional forms of spectroscopy.

TUNABLE DIODE LASERS

The diode lasers are fabricated from vapor-grown single crystals of $Pb_{1-x}Sn_xTe$ semiconducting material[10] by cleaving the crystals into rectangular parallelepipeds (each containing a p-n junction) of approximate overall dimensions $0.12 \times 0.05 \times 0.03$ cm. Low-resistance ohmic contacts are formed, and the laser is then mounted onto the cold-finger of a cryogenic Dewar. Liquid helium temperatures are presently required for continuous (cw) laser operation, with pulsed operation possible at liquid nitrogen temperature (77° K). The infrared emission frequency of the laser is, within the spontaneous emission bandwidth, determined by the refractive index of the semiconductor and the physical length of the cavity. This frequency can be fine-tuned by a small change in the d.c. diode current,[11] which alters the refractive index of this mixed-crystal semiconductor (which has low thermal conductivity) through heating. A single diode laser can be "tuned" in this manner over 40 cm^{-1} in continuous bands up to 2 cm^{-1} wide; but because of mode jumps at the ends of these bands, emission occurs at only about one-half the frequencies in this tuning range. Although continuous tuning is essential for fundamental high-resolution spectroscopic studies,[12] the broader, quasi-continuous tuning is quite adequate for application to pollutant gas detection. That the diode laser provides effectively infinite resolution for these applications was demonstrated by a heterodyne experiment involving a CO_2 laser,[13] where we showed that the linewidth of a 0.24 mW $Pb_{0.88}Sn_{0.12}Te$ diode laser at 10.6 μm was 54 kHz (1.8×10^{-6} cm^{-1}). By comparison, the narrowest Doppler-broadened linewidths of even the heaviest molecular pollutants are tens of MHz at room temperature.

APPLICATION TO POLLUTANT DETECTION

In a typical monitoring application, several $Pb_{1-x}Sn_xTe$ diode lasers would be used, each tailored to emit in a strongly absorbing infrared region of one of the pollutant gases. This is necessary because of the limited current-tuning range of these lasers, and desirable because it provides for increased specificity. The small size of these lasers permits several to be mounted into the same Dewar. Specific applications to pollutant detection can be divided into three categories: point-sampling, long-path atmospheric transmission, and remote emission sensing.

Point Sampling. This technique permits the absorption spectra to be measured at reduced pressure where possible overlap with neighboring spectral lines of the gas (or with other gases in the atmospheric sample) is minimized. Several experiments have been performed with $Pb_{0.88}Sn_{0.12}Te$ diode lasers in the 10.6 μm region to illustrate their usefulness in such an application. Figure D-1 shows absorption profiles of the strong sP(1,0) line of ammonia (NH_3) at several pressures. At low pressure the full linewidth at half peak absorption is seen to approximate the Doppler-limited value of 85 MHz. As the NH_3 pressure is increased toward 0.5 Torr, the 10-cm long cell becomes essentially opaque to radiation near the line center. The great improvement in sensitivity of this non-dispersive technique can be appreciated if a comparison is made between this spectrum and one obtained with a grating spectrometer having

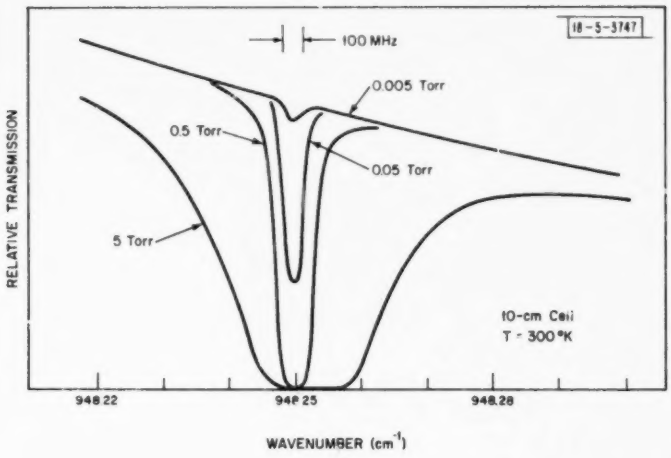

Fig. D-1. Absorption spectra of sP(1,0) line of NH_3 taken at various gas pressures with a tunable $Pb_{0.88}Sn_{0.12}Te$ diode laser. Resolution (diode laser linewidth) is better than 0.1 MHz (3.3×10^{-6} cm^{-1}).

0.1-0.2 cm^{-1} resolution.[14] In the latter experiment an NH_3 pressure of 5 Torr in a 200-cm long cell produced the same maximum absorption shown here for the 50 mTorr curve where the amount of NH_3 in the optical path is 2000 times smaller.

Figure D-2 shows the ν_3 vibration-rotation band of sulfur hexafluoride (SF_6) obtained with a high-quality grating spectrometer,[15] as well as a segment of this band taken with a tunable $Pb_{0.88}Sn_{0.12}Te$ diode laser. Since SF_6 is not usually present in the atmosphere, except near leakage sources such as high-voltage transformers, it can be used as a trace gas in certain monitoring applications.[16] Sulfur hexafluoride has an exceedingly complex spectrum in the infrared which, as shown in Fig. 2, cannot be resolved in the 950 cm^{-1} region even with a high-quality grating spectrometer, but is resolved by the diode laser scan. The widths of these lines correspond to the 29 MHz value predicted for Doppler broadening of SF_6 at room temperature, compared with 85 MHz for NH_3. Since a determination of mass can be made from the Doppler width, we can use tunable lasers to distinguish between gaseous species on the basis of their molecular weights, and thereby confirm pollutant identification by point-sampling at reduced pressure. The abscissa of Fig. 2 was precisely calibrated relative to the P(16) CO_2 line by the heterodyne/absorption technique described earlier.[12]

Ethylene (C_2H_4) is one of the many hydrocarbons present in automobile exhaust. It is not usually monitored separately, but is lumped with the others in a single measurement of total hydrocarbons. In Fig. D-3(a) is shown the absorption spectrum of C_2H_4 near the Q-branch of the ν_7 vibration-rotation band. The 25% drop in laser intensity near 949.24 cm^{-1} is produced by a shift of laser power from this longitudinal mode.[17] By modulating the diode current with a small (0.1%) superimposed sinusoidal current at a frequency of a few hundred Hz, the laser emission frequency is modulated; and, by synchronous detection, the derivative of the absorption spectrum is obtained. This is shown in Fig. D-3(b) where the top trace is a calibration spectrum of 1000 parts per million (ppm) C_2H_4 in N_2. A total gas pressure of 5 Torr produces a maximum derivative signal for C_2H_4, representing a balance between pressure-broadening

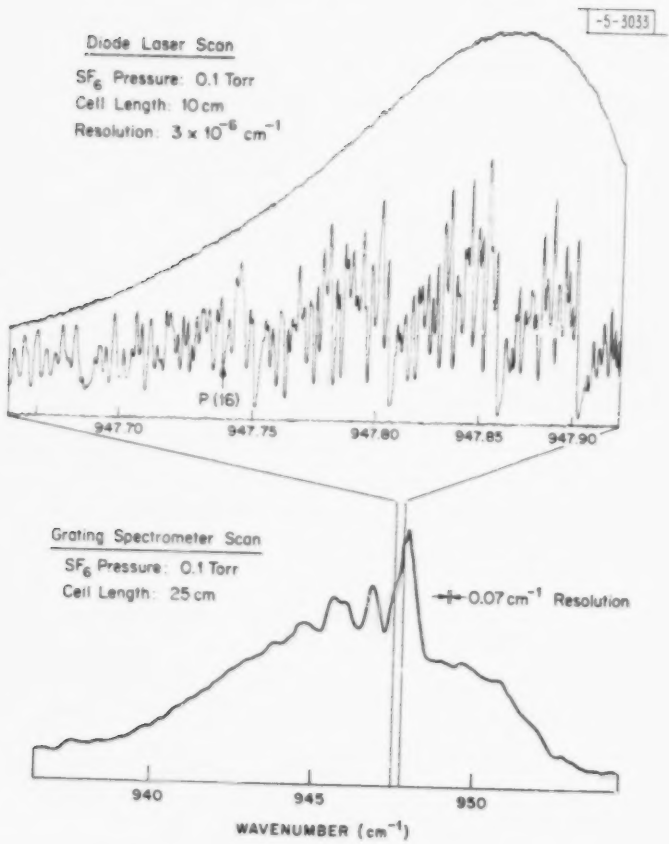

Fig. D-2. (Bottom) Grating spectrometer absorption curve of ν_3 band of SF_6 at room temperature. After Brunet and Perez.[15] (Top) Diode laser transmission scan of a segment of this band near the P(16) CO_2 laser line.

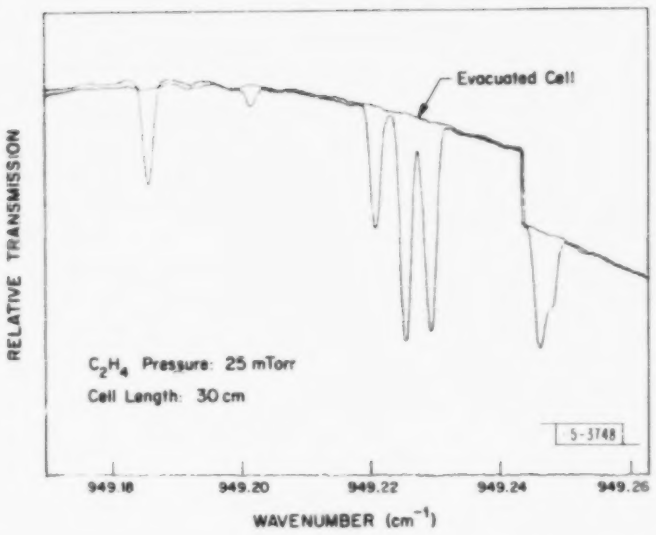

Fig. D-3(a). Absorption spectrum near the Q branch of C_2H_4 at 25 mTorr pressure. See Ref. (17) for experimental procedure.

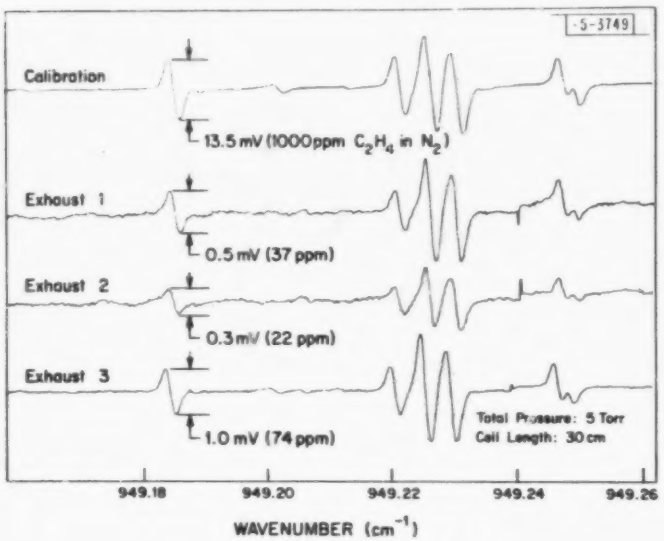

Fig. D-3(b). Derivative spectra of C_2H_4 calibration sample of 1000 ppm in N_2, and three automobile exhaust samples at different amplifier gain settings.

(upper limit) and reduced total number of absorbing molecules (lower limit). The lower three traces represent spectra obtained from automobile exhaust specimens, also taken at 5 Torr pressure, but with increased amplifier gain. By measuring the signal amplitudes and comparing them with the calibration curve, C_2H_4 concentrations of from 22 to 74 ppm are deduced. It is unmistakably clear that each automobile exhaust sample contains C_2H_4, and that there is no interference from water vapor or any other molecular constituents present. Moreover, the point at which the diode laser power changed abruptly is easily identifiable, and affects neither the qualitative nor the quantitative comparisons.

There is no question that this technique is very specific at low pressures where Doppler-broadening is predominant and collision-broadening negligible. Here each line is about 6×10^7 Hz (2×10^{-3} cm^{-1}) wide. The total (compositional) tuning range of the $Pb_{1-x}Sn_xTe$ diode lasers is about 3×10^{13} Hz. Assuming 50 gaseous molecular species in the atmosphere, each with 2000 reasonably strong lines in this range, the separation between individual lines should average about five times the linewidth.

The maximum absorption constant per unit pressure of the strongest lines of NH_3, SF_6, and C_2H_4 approximate 2 reciprocal centimeters per Torr. A detection limit of 0.3 ppm is expected for such lines in a 1-meter long cell on the basis of these initial experiments; but this limit should improve to the low parts-per-billion (ppb) range with the use of longer path-length, multiply reflecting cells, and improved electronics. Moreover, noting that the strengths of strong absorption lines of these three quite different gases are nearly equal, we expect those for a number of pollutant gases to have the same general values, yielding ultimate detection limits which are also in the low parts-per-billion range.

Long-Path Atmospheric Transmission. Even at atmospheric pressure the collision-broadened widths of spectral lines for typical gases are well below the resolution of infrared spectrometers presently available for field use. If a tunable diode laser is used, the resolution limit is imposed by the pressure-broadened linewidth of the gas itself, yielding all the available optical information within the tuning range. Monitoring of pollutant gases in the atmosphere by long-path transmission has the advantage over point sampling in that it produces an average value for the pollutant gas concentration over the path, which may be of greater overall significance in ambient air analysis.

If we assume that the pressure-broadened linewidth of the pollutant gas equals the Doppler width at about 5 Torr, and if we use a Doppler-broadened absorption constant per unit pressure of 2 reciprocal centimeters per Torr, the absorption constant (in reciprocal centimeters) at the center of a strong line at atmospheric pressure is

$$\alpha \approx 10^{-5} c \text{ cm}^{-1} , \qquad (1)$$

where c is the concentration in ppm. Over a one kilometer path, a pollutant gas with an average concentration of 1 ppb will produce a 0.1% change in transmission as we tune through this absorption line.

The collection efficiency will now be considered. The emitting area of the diode laser (which operates in a low-order transverse mode) is 500 μm × 40 μm. If a 20X beam expander is used, a laser beam near 10 μm wavelength diverges to an area of about 10^5 cm^2 one kilometer from the source. For a collection area of 100 cm^2 and a 1 W pulsed diode laser (tuned by varying either the pulse width or repetition rate), the collected power in the absence of attenuation is 1 mW. For an average pollutant concentration of 1 ppb over this path, a signal

change of 1 μW is produced – this can be measured easily using synchronous detection techniques. A corner reflector (of the order of 100 cm^2 or greater area to avoid diffraction losses in the return beam) situated remotely would eliminate the requirement of having instrumentation at two locations. By positioning a number of corner reflectors at various points around the source, many radial measurements could be made from the same monitoring station. It should also be pointed out that heterodyne detection of absorption lines, using an offset local oscillator, should yield an improved signal-to-noise ratio because of the narrow emission linewidth of the laser.

Transmission experiments should be performed with these diode lasers, operating both pulsed and cw, to test the feasibility of long-path monitoring, and to show whether or not specificity in identifying a particular gaseous pollutant can be retained in the presence of absorption lines from other molecular constituents. As is well known, H_2O and CO_2 have high abundances in the atmosphere and can cause serious interference with infrared spectroscopy. We, therefore, restrict ourselves to considering the 8-13 μm atmospheric "window," which is approximately 500 cm^{-1} wide. For example, lasers tailored to emit in the 8.6 μm region are better suited to sulfur dioxide (SO_2) detection than those tailored to the (somewhat stronger) 7.5 μm absorption band. Even in the "window" region, the wings of H_2O and CO_2 lines may produce greater absorption than that corresponding to pollutants in small concentrations; however, this is somewhat compensated by the fact that the slopes of these wings are relatively flat compared with the slope of a pollutant absorption line near its peak. Derivative spectroscopy, similar to that shown in Fig. D-3(b), will improve detection of these small peaks relative to the slowly varying Lorentzian wings of the dominant atmospheric absorption lines.

We now consider the interference between pollutant molecules at atmospheric pressure, and start with the assumption that there are 25 molecular species present which absorb in the 8-13 μm "window." At atmospheric pressure the lines are broadened to about 6×10^9 Hz, and most of the structure within individual J values of the P and R branches disappears – the Q branch, if present, also loses most of its structure since closely spaced strong lines overlap and weak lines become lost in the tails of strong lines. We estimate, therefore, that at atmospheric pressure there are only 100 resolvable lines per molecule, which implies that, on the average, the peaks of the lines are separated by one linewidth. Assuming each line is resolvable if a frequency interval three linewidths wide ($\sim 18 \times 10^9$ Hz) is not occupied by an absorption line from another molecule, and a uniform probability distribution, there should be an average of five resolvable lines per molecular specie.

Remote Emission Detection. One of the more difficult problems in air pollution monitoring is gaining access to industrial smokestacks. Optical remote-sensing techniques can be extremely useful for such applications.

Using the $Pb_{1-x}Sn_xTe$ diode laser as a tunable local oscillator, infrared heterodyne detection[18] of spectral emission lines from pollutants present in smokestack effluent may be performed.[19] (The technique is similar to that used by radio-astronomers to detect weak emissions from distant sources.) For heterodyne detection with an ideal photon counter (unit quantum efficiency and zero excess noise), the signal divided by the local-oscillator-generated noise is

$$\frac{S}{N} = \frac{1}{h\nu}\left(\frac{\partial P_s}{\partial \nu}\right)\sqrt{B\tau} \quad , \tag{2}$$

where $\partial P_s/\partial \nu$ is the received signal power per unit frequency range in a single spatial mode, $h\nu$ the infrared photon energy, B the intermediate-frequency (IF) bandwidth of the detection

system, and τ the post-detection integration time. For the case where the solid angle subtended by the source at the detector is larger than the diffraction-limited solid angular resolution of the collection optics – a situation usually valid for smokestack plumes at ranges up to 1 km with optics as small as 1 cm^2 – the signal-to-noise ratio becomes

$$\frac{S}{N} = (1 - e^{-\alpha L}) \left\{ \frac{1}{e^{h\nu/kT_s} - 1} - \frac{\epsilon_b}{e^{h\nu/kT_b} - 1} \right\} \sqrt{B\tau} \quad , \tag{3}$$

where L is the thickness of the plume and T_s its temperature, ϵ_b the emissivity of the background at temperature T_b, and k is Boltzmann's constant. We have assumed (a) that the IF bandwidth is less than the emission linewidth, (b) that the emission and absorption due to the pollutant in the ambient atmosphere is not important because of its low concentration relative to that in the plume, (c) negligible background attenuation from the wings of other molecular absorption lines, (d) that the local oscillator has sufficient power to overcome the other sources of noise (this is readily satisfied with a 1 mW diode laser). Note that since ϵ_b is often much smaller than unity (about 0.1 in the 10 μm region of the infrared when there are no clouds in the background) the source does not have to be hotter than the background, in fact, it could be colder. We choose the following representative values for the parameters: $B = 10^8$ Hz, τ = 1 sec, $\alpha = 10^{-5} c\ cm^{-1}$ (where c is the concentration in ppm), L = 1 meter, $h\nu$ = 0.125 eV, T_s = 400°K, T_b = 300°K, and ϵ_b = 1, to find

$$\frac{S}{N} \approx 0.2\, c \quad .$$

It should be possible, therefore, to remotely detect pollutant molecules such as SO_2 in smokestack plumes in concentrations greater than 10 ppm. In order to make absolute measurements of concentration, αL must be less than unity and the gas temperature must be known. If αL exceeds unity, so that the plume is optically dense, then a weaker emission line can be selected. Gas temperature can be measured in several ways: by heterodyne detection of one of the stack gases at two wavelengths, by performing multicolor broadband radiometric measurements, or by direct measurement at the top of the stack.

Atmospheric turbulence may cause fluctuations in the received signal. This can be overcome by alternately tuning the local oscillator between the peak emission wavelength of the pollutant gas and one of negligible emission in a time short enough so that turbulent effects are negligible (~1 millisecond), and then summing the excess pollutant signal for a large number of measurement intervals. Two local oscillators could also be used simultaneously – one operating at the emission peak, and the other offset from it.

GENERAL CONSIDERATIONS

The absorption bands of a few of the major molecular pollutant gases (such as CO and NO) are beyond the compositional tuning range of $Pb_{1-x}Sn_xTe$ diode lasers.[20] Development of other semiconducting materials, for example, $PbS_{1-x}Se_x$, which has produced laser emission under electron-beam excitation,[21] may yield tunable diode lasers useful for detecting these gases as well. Semiconductor lasers which operate in the 3-6.5 μm region should have the added advantage of a higher ultimate operating temperature.

Although temperatures below 20° K are presently required for continuous operation, pulsed laser emission can be obtained at liquid nitrogen temperature (77° K). With the availability of

relatively inexpensive cryogenic coolers, fast on-line monitoring of gases present in automobile exhausts or in chemical processing plants appears possible by direct absorption techniques using diode lasers, each of which is tailored to a strong absorption line of one of the gases to be monitored. It is expected that further improvements in materials fabrication will eventually permit cw operation at this temperature as well.

SUMMARY

Preliminary experiments indicate that tunable $Pb_{1-x}Sn_xTe$ diode lasers will be useful in the identification and sensitive detection of most of the atmospheric pollutant gases. For point-sampling applications, concentrations in the ppb range should be measurable with unsurpassed specificity. For long-range atmospheric transmission techniques, the improved resolution capability and tunability of these diode lasers make them attractive replacements for spectrometers and fixed-frequency laser sources where cryogenic temperature operation is not a serious impediment. By using these lasers as tunable local oscillators in the infrared heterodyne configuration, remote passive detection of gases present in smokestack effluent appears possible. Finally, pulsed operation at temperatures available with simple cryogenic coolers permits immediate application to fast detection of gases present in automobile exhaust and in chemical processing plants.

REFERENCES

1. A. R. Barringer, J. Opt. Soc. Amer. 60, 729 (1970); C. B. Ludwig, M. Griggs, and E. R. Bartle, ibid. 731 (1970).

2. H. J. Gerritsen, Trans. Amer. Inst. Mining Eng. 235, 428 (1966); G. B. Jacobs and L. R. Snowman, Inst. Elec. Electron. Eng. J. Quantum Electron. QE-3, 603 (1967); D. N. Jaynes and B. H. Beam, Appl. Opt. 8, 1741 (1969); P. L. Hanst, Appl. Spectrosc. 24, 161 (1970); R. T. Menzies, N. George, and M. L. Bhaumik, Inst. Elec. Electron. Eng. J. Quantum Electron. QE-6, 800 (1970).

3. H. Inaba and T. Kobayasi, Nature 224, 170 (1969); T. Kobayasi and H. Inaba, Appl. Phys. Lett. 17, 139 (1970).

4. Microwave spectroscopy has many of the advantages of optical spectroscopy for the detection of molecular pollutants, but with the following limitations: (i) insufficient resolution at atmospheric pressure; (ii) very low pressures required for high-resolution studies in the Doppler-limited regime, and (iii) molecules such as CO_2, C_2H_4, and C_6H_6, which lack a dipole moment in the ground state, cannot be detected.

5. J. O. Dimmock, I. Melngailis, and A. J. Strauss, Phys. Rev. Lett. 16, 1193 (1966); J. F. Butler, A. R. Calawa, and T. C. Harman, Appl. Phys. Lett. 9, 427 (1966); J. F. Butler and T. C. Harman, ibid. 12, 347 (1968); for a review, see I. Melngailis, J. Physique, Colloque C-4, Suppl. au no. 11-12 (1968), pp. C4-84 to C4-94 and T. C. Harman, J. Phys. Chem. Sol., in press.

6. J. M. Besson, J. F. Butler, A. R. Calawa, W. Paul, and R. H. Rediker, Appl. Phys. Lett. 7, 206 (1965); J. M. Besson, W. Paul, and A. R. Calawa, Phys. Rev. 173, 699 (1968).

7. J. F. Butler and A. R. Calawa, Physics of Quantum Electronics, edited by P. L. Kelley, B. Lax, and P. E. Tannenwald (McGraw-Hill, New York, 1966), p. 458; A. R. Calawa, J. O. Dimmock, T. C. Harman, and I. Melngailis, Phys. Rev. Lett. 23, 7 (1969).

8. E. D. Hinkley, M.I.T. Lincoln Laboratory Solid State Research Report, 1968:3, p. 19; T. C. Harman, A. R. Calawa, I. Melngailis, and J. O. Dimmock, Appl. Phys. Lett. 14, 333 (1969).

9. C. K. N. Patel and E. D. Shaw, Phys. Rev. Lett. 24, 451 (1970); A. Mooradian, S. R. J. Brueck, and F. A. Blum, Appl. Phys. Lett. 17, 481 (1970).

10. A. R. Calawa, T. C. Harman, M. Finn, and P. Youtz, Trans. Met. Soc. Amer. Inst. Mining Eng. 242, 374 (1968).

11. E. D. Hinkley, T. C. Harman, and C. Freed, Appl. Phys. Lett. 13, 49 (1968).

12. E. D. Hinkley, Appl. Phys. Lett. 16, 351 (1970).

13. E. D. Hinkley and C. Freed, Phys. Rev. Lett. 23, 277 (1969).

14. J. S. Garing, H. H. Nielsen, and K. Narahari Rao, J. Mol. Spectrosc. 3, 496 (1959).

15. H. Brunet and M. Perez, ibid. 29, 472 (1969).

16. A. Turk, S. M. Edmonds, H. L. Mark, and G. F. Collins, Environ. Sci. Technol. 2, 44 (1968).

17. A spectrometer has been inserted in front of the detector for the direct absorption experiments in order to measure the laser wavelength and to serve as a band-pass filter permitting radiation in a single longitudinal mode to be transmitted, while excluding that which may be simultaneously present in adjacent modes. In a field instrument this refinement is not necessary.

18. M. C. Teich, Proc. Inst. Elec. Electron. Eng. 56, 37 (1968).

19. R. H. Kingston, personal communication.

20. Although compositions with "x" approaching unity should produce lasers that emit near 3.7 micrometers at liquid helium temperatures, high carrier concentrations have, so far, thwarted attempts to produce such lasers (I. Melngailis, personal communication).

21. L. N. Kurbatov, A. D. Britov, I. S. Aver'yanov, V. E. Mashchenko, N. N. Mochalkin, and A. I. Dirochka, Soviet Physics – Semiconductors, 2, 1008 (1969).

22. We gratefully acknowledge the many technical contributions and continued encouragement of R. H. Kingston. Appreciation is expressed to T. C. Harman and A. R. Calawa for providing the $Pb_{1-x}Sn_xTe$ material and many of the diode lasers used in this work. We thank J. O. Sample and F. H. Caswell for laser fabrication and general technical assistance.

APPENDIX E
TUNABLE LASER SPECTROSCOPY OF THE ν_1 BAND OF SO_2*

E. D. Hinkley, A. R. Calawa, P. L. Kelley, and S. A. Clough†

Individual transitions of the ν_1 vibration-rotation band of SO_2 in the 8.7-μm wavelength region have been observed using tunable semiconductor diode lasers, and compared with theoretical calculations based on pure-rotation data from microwave absorption measurements. A new value of 1151.71 ± 0.01 cm^{-1} has been found for the ν_1 band center. Pressure-broadening coefficients and intensities of individual lines were determined from the high-resolution data, and a value was obtained for total band intensity.

The ν_1 band of SO_2 is composed of approximately 3000 relatively strong lines in the 1100- to 1200-cm^{-1} (9.1- to 8.3-μm) region. Using the high-resolution capability of tunable $Pb_{1-x}Sn_xTe$ diode lasers (linewidth less than 10^{-5} cm^{-1}), absorption spectra were obtained for 10 percent of these lines over various segments of the band.‡ The measured line positions and intensities are compared with those calculated using rotational constants of Steenbeckeliers derived for both the (000) and (100) vibrational states from accurate microwave absorption data.[2] In the calculation, energy levels and eigenvectors were determined for rotational quantum numbers J to 60, and the rotational partition sum was evaluated and found to be Q_R = 5805 at 296°K. Transition frequencies and strengths corresponding to $\Delta J = 0, \pm 1$ and $\Delta K_A = \pm 1, \pm 3$ were then evaluated, yielding positive identification of over 95 percent of the observed lines.

In order to produce diode lasers which emit between 1100 and 1200 cm^{-1}, single crystals of $Pb_{1-x}Sn_xTe$ were grown[3] at three different compositions: x = 0.0575, 0.0700, and 0.0745. The crystals were cleaved into rectangular parallelepipeds (each containing a p-n junction) of average size 0.084 × 0.025 × 0.020 cm. Fine tuning of the wavelength within a single longitudinal mode was achieved by changing the diode current, which alters the refractive index of the semiconductor through heating of the junction region. Each of the six diode lasers used for this study exhibited continuous power in the 6- to 44-μW range at 500 A/cm^2. Absorption spectroscopy was performed by transmitting the tunable laser radiation through a 30-cm-long cell containing SO_2, using techniques described earlier.[4] The SO_2 was obtained from the Matheson Company, Inc. of East Rutherford, New Jersey, with a quoted purity of 99.98 percent. Gas pressure was measured with a capacitance manometer below 1 Torr, and with a Wallace-Tiernan gauge at higher pressures.

Figure E-1 shows 1.4-cm^{-1}-wide scans, between 1156.3 and 1157.7 cm^{-1}, of SO_2 at pressures of 0.1, 1, and 10 Torr, in addition to one of NH_3 which yielded two lines for wavelength calibration. The 10-Torr curve shows definite pressure-broadening and overlap of closely

---

* Submitted for publication.

† Air Force Cambridge Research Laboratories.

‡ In earlier work,[1] a single PbSnTe diode laser was temperature-tuned over the entire ν_1 band of SO_2, however, individual transitions were not observed.

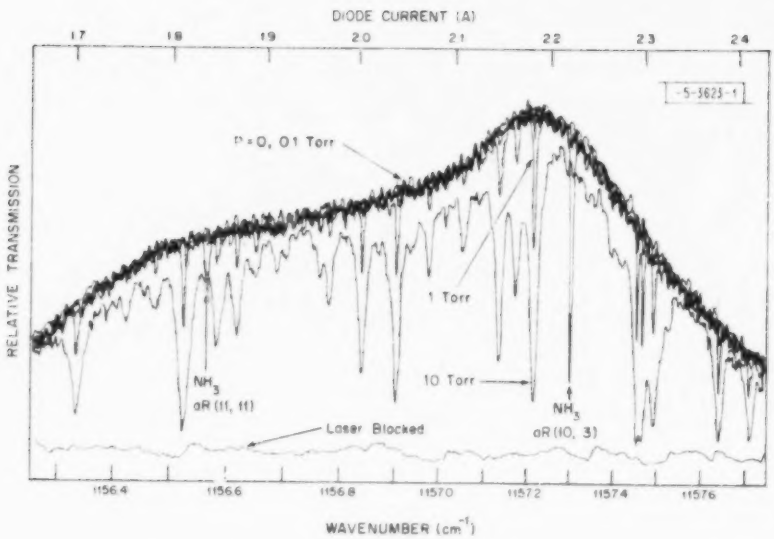

Fig. E-1. Diode laser scans of SO_2 at pressures of 0, 0.1, 1, and 10 Torr at room temperature with a 30-cm cell. The NH_3 lines were taken at 1-Torr pressure. Diode laser excitation (and tuning) current is shown by the upper horizontal scale. Eighteen of these SO_2 lines have been identified: some of the strongest are $18_{2,16} \leftarrow 18_{1,17}$ (1156.523 cm^{-1}), $10_{0,10} \leftarrow 9_{1,9}$ (1156.911 cm^{-1}), $22_{3,19} \leftarrow 22_{2,20}$ (1157.442 cm^{-1}), $24_{3,21} \leftarrow 24_{2,22}$ (1157.455 cm^{-1}).

spaced lines which are resolved at lower pressures. (Absorption at 0.1 Torr is difficult to see because of the high noise level of this particular set of scans.) Individual SO_2 transitions were identified by comparing their relative positions and intensities with theory. Using the latest values for NH_3 line positions in this region[5] to calibrate the more than twenty segments covered between 1110 and 1170 cm^{-1}, we obtain a value of 1151.71 ± 0.01 cm^{-1} for the ν_1 band center frequency of $^{32}S^{16}O_2$, which can be compared with 1151.38 cm^{-1} of Shelton, Nielsen, and Fletcher.[6]

Figure E-2 represents a detailed comparison in the 1147-cm^{-1} region between results of a diode laser scan and the theoretical intensities and positions of lines in this region. The curves are Lorentzian fits to the intensities, incorporating a linewidth which best reproduces the shape of the experimental curve at 1-Torr pressure. (At this pressure, the SO_2 line profile is actually a convolution of Gaussian and Lorentzian lines whose widths are comparable.) Minor differences between the two curves are indicated at a, b, and c, where transitions involving higher values of J and K_A (relative to adjacent lines) are noticeably shifted from their calculated positions. At d is a line which is not predicted; this may be due to a "hot" band transition, other isotope, or weaker transition not included in the calculation.

The very high resolution made possible by these tunable lasers permits essentially undistorted measurements of individual line profiles, so that pressure-broadening studies can be carried out by direct linewidth measurements. Figure E-3 illustrates the effects of increased pressure on the widths of two SO_2 lines. At pressures above a few Torr, self-broadening of the $15_{4,12} \leftarrow 15_{3,13}$ line occurs at a rate of 20 ± 3 MHz/Torr for the half-width at half-maximum.

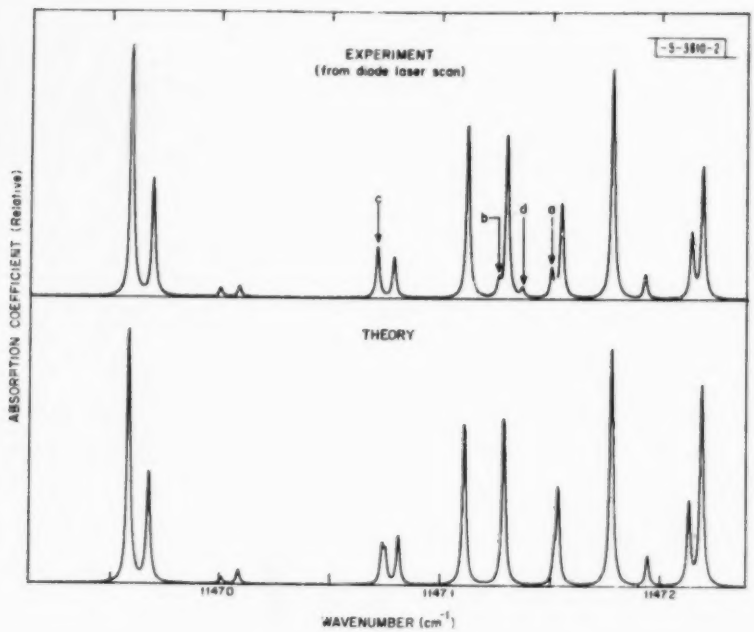

Fig. E-2. Comparison between measured and calculated absorption coefficients and positions for some lines in the ν_1 band of SO_2. These scans were computer-generated using Lorentzian profiles. Lines designated as a, b, and c represent the transitions $^{29}_{6,24} \leftarrow {}^{28}_{7,21}$, $^{35}_{7,29} \leftarrow {}^{34}_{8,26}$, and $^{26}_{4,22} \leftarrow {}^{27}_{3,25}$, respectively. Line d is not predicted by theory.

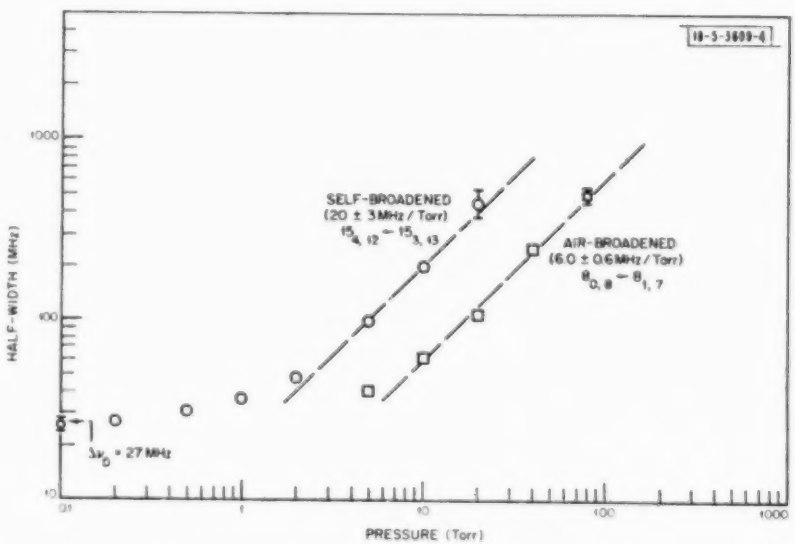

Fig. E-3. Self-broadened and air-broadened dependence of the half-width at half-maximum intensity for two lines at room temperature: $^{15}_{4,12} \leftarrow {}^{15}_{3,13}$ at 1163.297 cm^{-1}, and $^{8}_{0,8} \leftarrow {}^{8}_{1,7}$ at 1148.849 cm^{-1}.

The effect of air-broadening is shown for the $8_{0,8} \leftarrow 8_{1,7}$ transition, where the rate is 6.0 ± 0.6 MHz/Torr, or 3.3 ± 0.6 times smaller than for self-broadening of the other transition. Similar measurements on other lines do not show any large deviation from the rates shown here. Our measured ratio between self-broadening and air-broadening rates can be compared with a value of 5 ± 1 obtained by Burch, et al.,[7] using a broadband technique and dry nitrogen instead of air.

The intensities of several rather isolated SO_2 lines were determined from their peak absorption constants and linewidths at a pressure of 10 Torr. Table I lists the transitions, their measured intensities, and projected values for the total ν_1 band intensity obtained by dividing the measured intensity of each line by its calculated fractional contribution to the band. Averaging these values yields a total ν_1 band intensity of $358 \pm 20 \times 10^{-20}$ cm^{-1} molecule^{-1} cm^2, which is comparable with a value of $371 \pm 20 \times 10^{-20}$ cm^{-1} molecule^{-1} cm^2 recently obtained by Burch, et al,[7] and within the range quoted by earlier workers,[8-10] employing the integrated band technique. Using our result, the effective vibrational transition moment for the ν_1 fundamental is found to be

$$|\mu_{ij}| = 0.086 \pm 0.003 \text{ Debye} \quad .$$

TABLE I

MEASURED INTENSITIES OF $^{32}S^{16}O_2$ TRANSITIONS AND PROJECTED ν_1 BAND INTENSITY

Transition* $J'_{K'_A,K'_C} \leftarrow J''_{K''_A,K''_C}$	Frequency (cm^{-1})	Measured Intensity ($cm^{-1}molec^{-1}cm^2$)	Projected Total Band Intensity ($cm^{-1}molec^{-1}cm^2$)
$30_{10,20} \leftarrow 30_{11,19}$	1115.031	0.66×10^{-21}	351×10^{-20}
$23_{5,19} \leftarrow 24_{6,18}$	1116.962	1.44	392
$18_{6,12} \leftarrow 19_{7,13}$	1117.038	1.67	356
$13_{7,7} \leftarrow 14_{8,6}$	1117.128	1.96	367
$22_{9,13} \leftarrow 22_{10,12}$	1118.956	1.04	354
$8_{0,8} \leftarrow 8_{1,7}$	1148.810	2.96	332
$6_{0,6} \leftarrow 6_{1,5}$	1149.346	2.74	336
$2_{1,1} \leftarrow 2_{0,2}$	1153.488	1.43	368
$5_{1,5} \leftarrow 4_{0,4}$	1156.195	1.86	384
$14_{1,13} \leftarrow 14_{0,14}$	1156.842	2.51	336

* Conventional spectroscopic notation is followed, where the upper state is listed first.

ACKNOWLEDGMENTS

We are pleased to acknowledge the help of W. F. McBride and A. Wilson in diode laser fabrication, J. O. Sample and T. E. Stack for performing the many spectroscopic measurements. Appreciation is also expressed to Professor K. N. Rao and his associates at the Ohio State University for prepublication values of the NH_3 line positions.

REFERENCES

1. P. Norton, P. Chia, T. Braggins, and H. Levinstein, Appl. Phys. Lett. 18, 158 (1971).
2. G. Steenbeckeliers, Ann. Soc. Sci., Bruxelles 82, 331 (1968). Calculations were performed in the manner of W. S. Benedict, S. A. Clough, L. Frenkel, and T. E. Sullivan, J. Chem. Phys. 53, 2565 (1970).
3. A. R. Calawa, T. C. Harman, M. Finn, and P. Youtz, Trans. Met. Soc. AIME 242, 374 (1968).
4. E. D. Hinkley, Appl. Phys. Lett. 16, 351 (1970). See also E. D. Hinkley and P. L. Kelley, Science 171, 635 (1971).
5. K. N. Rao, J. B. Curtis, and P. Yin (private communication). The NH_3 transitions are identified using the notation of J. S. Garing, H. H. Nielsen, and K. N. Rao, J. Molec. Spectry. 3, 496 (1959).
6. R. D. Shelton, A. H. Nielsen, and W. H. Fletcher, J. Chem. Phys. 21, 2178 (1953).
7. D. E. Burch, J. D. Pembrook, and D. A. Gryvnak (prive communication).
8. J. Morcillo and J. Herranz, Anales real Soc. espan. fis. y quim. A 52, 207 (1956).
9. J. E. Mayhood, Can. J. Phys. 35, 954 (1957).
10. D. F. Eggers, Jr. and E. D. Schmid, J. Phys. Chem. 64, 279 (1960).